Water Research 281 (2025) 123679

Contents lists available at ScienceDirect

Water Research

journal homepage: www.elsevier.com/locate/watres

Magnetic activated carbon for improving the removal of antibiotics by heterogeneous solar photo-Fenton at circumneutral pH

Karla V.L. Lima [a], Raquel F. Pupo Nogueira [a], Érika M.L. Sousa [b], Mário M.Q. Simões [c], Diana L.D. Lima [d,*], Vânia Calisto [b]

[a] São Paulo State University (UNESP), Institute of Chemistry, 14800-060 Araraquara, SP, Brazil
[b] CESAM, Department of Chemistry, University of Aveiro, 3810-193 Aveiro, Portugal
[c] LAQV-REQUIMTE, Department of Chemistry, University of Aveiro, 3810-193 Aveiro, Portugal
[d] H&TRC - Health & Technology Research Center, Coimbra Health School, Polytechnic University of Coimbra, Rua 5 de Outubro, 3045-043 Coimbra, Portugal

ARTICLE INFO

Keywords:
Waste-based material
Sulfamethoxazole
Trimethoprim
Photodegradation
Solar radiation
Reuse

ABSTRACT

A pulp and paper industry waste-based powder activated carbon combined with Fe nanoparticles (PAC-Fe) was obtained through a simple one-step synthesis for application in heterogeneous photo-Fenton treatment. PAC-Fe was characterized and applied for the removal of sulfamethoxazole (SMX) and trimethoprim (TMP) from water at circumneutral pH and under simulated solar irradiation. The contribution of the different processes involved in the overall removal of the contaminants (adsorption, Fenton and photo-Fenton) was evaluated. Degradation in both Fenton and photo-Fenton processes were fitted to the pseudo first-order and BMG kinetic models. Photo-Fenton resulted in the complete removal of SMX and TMP from water within 20 min. In contrast, in the absence of the material (H_2O_2 + UV), only 49 % and 59 % of SMX and TMP were removed, respectively, after the same time. The synthesis procedure allowed to obtain a PAC-Fe with a satisfactory saturation magnetization (21.14 emu g^{-1}) and stability without any detectable leaching of iron during its application. The magnetic properties of PAC-Fe allowed for easy separation from the treated water, with degradation percentage above 50 % and 70 %, for SMX and TMP, respectively, after five consecutive cycles. The removal mechanisms involved a combination of different processes, with heterogeneous photo-Fenton and Fenton proving to be the most significant, followed by adsorption and photo-assisted peroxidation to a smaller extent. Eight transformation products of SMX were identified and fourteen for TMP, which were formed mainly by hydroxylation. The results achieved at pH close to neutral show that the PAC-Fe can be relevant for application in wastewater treatment.

1. Introduction

The presence of antibiotics in the environment, recognized as important emerging contaminants, is a matter of global concern due to the potential for the development of antibiotic-resistant genes and creation of superbugs (Ahmed et al., 2015). Despite the efforts of current wastewater treatment facilities, they are not able to effectively remove antibiotics from sewage (Wang et al., 2021). The antibiotics sulfamethoxazole (SMX) and trimethoprim (TMP) have been commonly detected in different aqueous matrices, including Wastewater Treatment Plant (WWTP) effluents, in concentrations ranging from 0.019 ng L^{-1} to 1820 ng L^{-1} (Sanusi et al., 2023). In 2022, SMX and TMP have been included on the list of priority pharmaceuticals to receive global attention (Yang et al., 2022). In addition, they are listed in the latest Watch List of the Commission Implementing Decision (EU) 2022/1307 of 22 July 2022, as substances requiring monitoring in waters (EC 2022). As a result, there is a pressing need for the development of new and cost-effective technologies aiming at the removal of such antibiotics from municipal wastewaters to prevent aqueous environment contamination and development of bacterial resistance.

Several methods have been studied for removing SMX and TMP from water, including adsorption (Sousa et al., 2022), membrane separation (Song et al., 2023), biological treatment (Özel Duygan et al., 2021), and advanced oxidation processes (AOPs) (Serna-Galvis et al., 2019). Adsorption is a simple and efficient process, but high regeneration costs of saturated/contaminated adsorbents through thermal or chemical methods might offset its advantages (Salvador et al., 2015), while membrane separation is efficient but prone to fouling problems,

* Corresponding author.
E-mail address: diana.lima@estesc.ipc.pt (D.L.D. Lima).

https://doi.org/10.1016/j.watres.2025.123679
Received 31 January 2025; Received in revised form 3 April 2025; Accepted 18 April 2025
Available online 19 April 2025

affecting its stability (Bokhary et al., 2018). Biological methods are considered slow and provide low removal of antibiotics (Liu et al., 2018). AOPs are highly effective in breaking down several organic pollutants mediated by free radicals (Badmus et al., 2018). One of the most used AOPs is the Fenton process, which has been widely applied to eliminate antibiotics, including SMX (Soriano-Molina et al., 2021) and TMP (Martínez-Costa et al., 2018), from water samples. This process generates hydroxyl radicals ($HO^{\bullet}$), which have high redox potential to induce degradation of organic molecules (Li et al., 2022). In the Fenton process, this radical is generated by the reaction between hydrogen peroxide (H_2O_2) and Fe^{2+}, which is initially oxidized to Fe^{3+} (Eq. (1)). The Fe^{2+} regeneration (Eq. (2)) is the slowest and most limiting stage of the process. So it is common to combine the Fenton process with UV/Vis radiation (photo-Fenton process), which induces a charge transfer process from the ligand to the metal through the photolysis of Fe(III) aquacomplexes (Eq. (3)). The Fe^{2+} generated reacts with H_2O_2, promoting a continuous cycle of $HO^{\bullet}$ generation. Furthermore, UV irradiation can also induce the photolysis of H_2O_2 generating $HO^{\bullet}$ (Eq. (4)) (Bokare and Choi, 2014).

$$Fe^{2+} + H_2O_2 \rightarrow Fe^{3+} + HO^{\bullet} + HO^{-} \ (k = 63 - 76\ M^{-1}\ s^{-1}) \quad (1)$$

$$Fe^{3+} + H_2O_2 \rightarrow Fe^{2+} + HO_2^{\bullet} + H^{+} \ (k = 0.001 - 0.01\ M^{-1}\ s^{-1}) \quad (2)$$

$$Fe(OH)^{2+} + h\nu \rightarrow Fe^{2+} + HO^{\bullet} \quad (3)$$

$$H_2O_2 + h\nu \rightarrow 2HO^{\bullet} \quad (4)$$

Although efficient in the degradation of organic compounds, homogeneous Fenton or photo-Fenton processes can result in the production of a large amount of iron sludge that cannot be reused, leading to additional costs related to waste disposal (Jiang et al., 2022). The homogeneous process is highly dependent on the pH of the medium, as at values above 4 formation of Fe(III) precipitates occur, compromising the efficiency of the process. As a result, efforts have been made to develop heterogeneous photo-Fenton-based processes, which utilize Fe-based solid catalysts that can be applied at circumneutral pH (Bokare and Choi, 2014; Hussain et al., 2021).

In the heterogeneous process, the catalyst is mainly composed of Fe (III), stabilized within its structure, allowing it to react with H_2O_2 and generate $HO^{\bullet}$ without forming iron hydroxide precipitates. The Fe(III)/Fe(II) redox cycle is crucial for maintaining continuous activity, but, similar to the homogeneous process, the reduction of Fe(III) by H_2O_2 is the rate-limiting step, affecting the overall efficiency. Additionally, H_2O_2 decomposition produces hydroperoxyl radicals ($HO_2^{\bullet}$), which are less reactive than $HO^{\bullet}$, potentially reducing process effectiveness. Accelerating the Fe(III)/Fe(II) redox cycle and optimizing H_2O_2 utilization remain key challenges, driving the development of heterogeneous Fenton catalysts that overcome these limitations, expand the pH range, and exhibit greater stability (Zhu et al., 2019).

Several iron-loaded solid catalysts have been developed by attaching iron to solid supports for use in Fenton-based oxidation, such as chalcopyrite (Labiadh et al., 2019), carbon materials (graphene, carbon nanotubes, biochar, and powder or granular activated carbon) (He et al., 2022; Pan et al., 2019). Among carbon materials, activated carbon (AC) is seen as a low-cost and environmentally friendly support for heterogeneous Fenton catalysts when obtained from residual feedstocks, like agricultural and industrial wastes (Sousa et al., 2022; Shang et al., 2016; Cao et al., 2021; Brazil et al., 2022). In this context, industrial paper mill waste, which is generated in large volumes worldwide (one ton of paper generates 40–50 kg of dry sludge, of which 70 % is primary sludge (Bajpai, 2015)), presents a promising raw material for the large-scale production of AC, offering a sustainable alternative for catalyst support while addressing waste disposal challenges. By combining Fe nanoparticles and powder activated carbon (PAC), it is possible to create a powder magnetic activated carbon-based (PAC-Fe) composite. This composite offers several benefits, such as a large specific surface area and active sites. These advantages can enhance the effectiveness of Fenton-based processes by enabling the immobilization of iron species onto a solid matrix, keeping the iron available for the Fenton-process (Seidmohammadi et al., 2021). In addition, the magnetic properties of these composites facilitate their separation from the solution at the end of the process and their reuse.

Some studies have reported the impregnation of iron onto carbon surfaces for antibiotic removal via Fenton or photo-Fenton processes. Jaafarzadeh et al. used PAC combined with magnetite, synthesized by coprecipitation, for tetracycline degradation, however it was more effective in acidic medium (pH 3–5) (Jaafarzadeh et al., 2015). Another study investigated the removal of six tetracycline-class antibiotics using granular AC loaded with iron (GAC-Fe). The catalyst showed promising performance at pH 7 for some of the antibiotics but evidenced instability, leading to iron leaching. The iron concentration in solution reached a maximum of 0.15 mg L^{-1} at the end of the experiments with 0.3 g L^{-1} of the catalyst, and the homogeneous Fenton process contributed to antibiotic degradation (Pan et al., 2019). A different GAC-Fe composite also demonstrated higher efficiency for tetracycline degradation at pH 3 (He et al., 2022). Li et al. (2021) studied the degradation of ciprofloxacin, norfloxacin, and ofloxacin using organic carbon modified with schwertmannite loaded with magnetite, showing applicability in a pH range of 2–8 . Carbon-based materials have also been employed for the degradation of SMX, e.g. Tang and Wang (2018), incorporated magnetic Fe nanoparticles into mesoporous carbon , Zeng and Kan (2022) used biochar activated with $FeCl_3$, while Zárate-Guzmán et al. (2020), employed GAC as a support for iron . However, as observed in most studies applying carbon-iron composites, these catalysts were more efficient in acidic conditions (pH < 4), limiting their real-world applicability.

To the best of the authors' knowledge, no study has yet investigated the degradation of SMX and TMP using PAC-Fe catalyst under solar irradiation, nor have the degradation pathways of these antibiotics in such system been explored. Also, traditional methods for synthesizing PAC-Fe heterogeneous Fenton catalysts often require a two-step process, including the production of AC, through chemical activation and pyrolysis, followed by the attachment of Fe compounds, which is time-consuming and energy-intensive. In contrast, this study presents a more efficient one-step synthesis, combining activation and iron fixation on the surface of AC simultaneously, which represents an interesting advancement in streamlining the production of such catalysts (Zeng and Kan, 2022). Although the one-step synthesis of PAC-Fe from paper mill sludge has been reported once in the literature, its application was focused on adsorption (Pereira et al., 2025). Considering these gaps, the goals of this study were to: (1) synthesize, via one-step procedure, and characterize a PAC-Fe nanocomposite; (2) study the degradation of SMX and TMP in a heterogeneous solar photo-Fenton process at circumneutral pH using the PAC-Fe nanocomposite prepared in the previous step, including the effect of catalyst amount; (3) evaluate catalyst reuse cycles; and (4) identify the transformation products generated during the degradation process and suggest possible degradation pathways for SMX and TMP.

2. Materials and methods

2.1. Reagents

The antibiotics SMX (≥98.0 %) and TMP (≥98.0 %) were provided by Tokyo Chemical Industry Co., Ltd. (TCI). Hydrogen peroxide (H_2O_2 - 30.0 %) and formic acid (≥98.0 %) were provided by Sigma Aldrich. Methanol (≥99.8 %) and hydrochloric acid (HCl - 37 %) were obtained from Fisher Chemical. Iron (III) chloride ($FeCl_3$ - 99.0 %) was purchased from Chem Lab. Potassium hydroxide (KOH - 85.0 %) was obtained from Lab Kem. Sodium hydroxide (NaOH - 99.3 %) was obtained from José Manuel Gomes dos Santos (Portugal). Ammonium metavanadate (≥99.0 %) was purchased from Panreac Applichem. All the solutions were

prepared in ultrapure water obtained from a PURELAB Flex 4 system (Elga, Veolia).

2.2. Preparation of PAC-Fe catalyst

Primary paper mill sludge resulting from primary wastewater treatment applied in a pulp and paper industry was used as PAC precursor. The pulp and paper mill industry employs a kraft elemental chlorine-free production process and utilizes *eucalyptus globulus* wood. After collection, the precursor was air-dried at room temperature and subsequently heated at 105 °C for 24 h in an oven, and then, grounded with a blade mill to obtain fine particles (Jaria et al., 2019).

The PAC-Fe catalyst was produced by a one-step synthesis, which is an easy and potentially cost-reducing process that combines chemical activation and Fe incorporation into a single step. For that purpose, the precursor was subjected to a simultaneous impregnation with KOH and $FeCl_3$ (precursor:$FeCl_3$:KOH ratio 5:5:1 *w/w*). Then, the mixture was sonicated for 1 h. The resulting slurry was air-dried for several days and was then pyrolyzed in an industrial microwave furnace (Phoenix™ AirWave CEM) under N_2 atmosphere at a temperature of 600 °C for 20 min (heating rate of 15 °C min^{-1}). After carbonization, 44.95 g of the material were maintained in contact with 1.5 L of 0.5 M HCl for 1 h. Then, the material was washed with distilled water until the washing solution presented a neutral pH and then dried at 50 °C overnight. The resulting PAC-Fe was manually ground and finally sieved to obtain a particle size $\leq$ 180 μm.

2.3. PAC-Fe characterization

X-ray diffraction (XRD) measurements were conducted at room temperature using a Panalytical Empyrean powder diffractometer. Monochromated CuKα radiation ($\lambda = 1.541°$ A) was utilized in the 10 to 80° 2θ range at 0.02° resolution with 4000 acquisition points per step.

The zeta potential was determined as a function of pH (adjusted with 0.05 M HCl or NaOH) at 25 °C measured using a Zetasizer Nano ZS90 system from Malvern Instruments. All the analyses were performed in triplicate at the pH range from 3 to 9. This pH range was selected due to its relevance to the study conditions, particularly for PAC-Fe application in water treatment under circumneutral pH.

SEM was performed to obtain surface images before and after the use of PAC-Fe in the photocatalysis experiments, using a field emission scanning electron microscope (model 7500F, JEOL) operating at an accelerating voltage of 2 kV.

The chemical surface analysis of PAC-Fe, both before and after application in the photo-Fenton process, was conducted through X-ray photoelectron spectroscopy (XPS). The XPS analysis was carried out in a conventional XPS K-Alpha model, from Thermo Scientific with Al Ka radiation ($h\nu = 1486$ eV) as the excitation source. The XPS spectra were recorded at a constant pass energy of 200 eV with a 1 eV per step for survey spectra and pass energy of 50 eV with a 0.1 eV per step for high-resolution acquisition. The analysis of the XPS spectra was performed using the CASA XPS software.

The textural properties of the PAC-Fe (specific surface area (S_{BET}) and porosity) were analyzed using a Micromeritics ASAP 2420 instrument coupled with N_2 adsorption isotherm at -196 °C. The Brunauer-Emmett-Teller equation was applied to the relative pressure range of 0.01–0.1 to determine the S_{BET}. The total micropore volume (W_0) was calculated using the Dubinin-Astakhov equation, while the total pore volume (V_p) was estimated from the amount of N_2 adsorbed at a relative pressure of 0.99. The average pore width (D) was determined assuming slit-shaped pores and calculated as 2 times the ratio of V_p to S_{BET}.

A Vibrating-sample magnetometer (VSM) EV9 instrument with an oscillatory magnetic field was utilized to conduct magnetization measurements at room temperature, with the maximum applied magnetic field (H) reaching 22 kOe. The saturation magnetization (*Ms*) was determined by plotting the magnetic moment against the applied magnetic field. The *plateau* value of the magnetic moment was divided by the sample mass (10 mg) to obtain M_S. Prior to analysis, the instrument was calibrated using a pure nickel disk (8 mm diameter) to establish magnetic field determination at approximately 1 Oe, while ensuring that the magnetic moment dispersion (m) was below 0.5 %.

2.4. Chromatographic analysis

The quantification of SMX and TMP in the aqueous phase was carried out by high-performance liquid chromatography (HPLC) using a Waters Alliance 2695 Separation Module with a Waters 2487 Dual Absorbance detector, equipped with a UV/visible detection system, and operated with the software Empower 3. The separation was achieved on a 150 mm × 4.6 mm i.d. ACE® C18 column-PFP (5 μm particle size) connected to a 4.6 mm i.d. ACE®5 C18 guard column. The mobile phase consisted of 25:75 (*v/v*) 0.1 % formic acid: methanol at a flow rate of 0.8 mL min^{-1}. The mobile phase was filtered through a 0.2 μm polyamide membrane filter (Whatman) prior to use. The injection volume was 60 μL, and detection was monitored at 270 nm. Prior to analysis, all the samples were filtered with a polyvinylidene fluoride (PVDF) filter with a 0.22 μm pore size (Whatman).

Standard stock solutions of 100 mg L^{-1} SMX and TMP were prepared and subsequently diluted in ultrapure water to reach the desired concentration for the degradation experiments. The calibration curves of SMX and TMP were obtained by analyzing standard solutions in the linear range of 50–1000 μg L^{-1} for SMX and 50–800 μg L^{-1} for TMP. All the samples and solutions were analyzed in triplicate. Additional details about the calibration curve can be found in the supplementary material (SM).

2.5. Heterogeneous solar photo-Fenton experiments

A Solarbox 1500 (Co.fo.me.gra, Italy) equipped with an arc xenon lamp (1500 W) was used to perform all degradation experiments. This source of irradiation provides the most accurate artificial reproduction of the solar energy distribution at the Earth's surface in the 290–700 nm wavelength range (Finlayson-Pitts and Pitts, 2000), using UV filters that limit the transmission of light < 290 nm. The experiments were performed under a constant irradiation level of 55 W m^{-2} (290–400 nm), measured using a multimeter with a UV 290–400 nm band sensor, also from Co.fo.me.gra. To ensure uniform irradiation within the chamber, a parabolic reflection system was employed. The temperature inside the chamber was kept at 30 ± 2 °C using an air-cooling system.

All the batch heterogeneous photo-Fenton tests were conducted in a glass beaker (7.0 cm internal diameter and 9.7 cm height) by adding H_2O_2 (5.0 mM) to 250 mL of a solution containing 200 μg L^{-1} of both SMX and TMP. This concentration was chosen to ensure reliable analytical quantification of TPM and SMX during the experiments. The pH of the antibiotic solution was adjusted to 8.1 ± 0.1, with 0.1 M NaOH, measured with a pH meter (model HANNA HI2221). The importance of this pH value lies in the applicability of the process to wastewater treatment, as it closely reflects the pH levels normally found in urban effluents. After adjusting the pH and adding H_2O_2, the catalyst PAC-Fe was introduced, and the solution was maintained under magnetic stirring (350 rpm) throughout the experiment.

2.5.1. Selection of PAC-Fe amount

To evaluate the effect of the PAC-Fe amount on the photo-Fenton degradation of SMX and TMP and to select the operational condition for further studies, experiments were carried out varying the PAC-Fe amount (0.10, 0.25, 0.35 and 0.50 g L^{-1}). For each catalyst amount, a 10-min photo-Fenton test was performed, during which the initial and final concentrations of antibiotics were analyzed to calculate the removal (%). The 10-min duration was selected based on preliminary experiments, which demonstrated that with 0.25 g L^{-1} of PAC-Fe 10 min were adequate to achieve over 50 % removal of both antibiotics.

The removal (%) for each antibiotic was determined according to Eq. (5).

$$\text{Removal } (\%) = \left(1 - \frac{C}{C_0}\right) x100 \quad (5)$$

where C is the concentration (μg L^{-1}) of each antibiotic at a given irradiation time and C_0 corresponds to its initial concentration.

The stability of the material was assessed by determining the iron leached from different PAC-Fe amounts tested. The solutions were filtered and analyzed using atomic absorption (Perkin Elmer, AAnalyst 100), with a limit of detection (LOD) of 0.09 mg L^{-1}. The H_2O_2 content in solution at the end of the experiment was determined according to Nogueira et al. (2005).

2.5.2. Evaluation of antibiotic removal through different processes

A pre-defined set of experiments were performed to evaluate the contribution of other processes in the removal of each antibiotic under study. Apart from photo-Fenton process, the removal of antibiotics by adsorption (only PAC-Fe, no light and no H_2O_2), photolysis (with light, but no PAC-Fe and no H_2O_2), photocatalysis (PAC-Fe + light, no H_2O_2), photo-assisted peroxidation (H_2O_2 + light, but no PAC-Fe) and Fenton (PAC-Fe + H_2O_2, but no light) processes were also studied. In experiments involving PAC-Fe, the catalyst amount used was chosen after studying the PAC-Fe amount effect, as described in Section 2.5.1. All experiments were performed over 20 min. However, the percentage of antibiotic removal after 15 min was adopted to compare the contribution of each process.

2.5.3. Kinetic of antibiotics removal from aqueous samples

For kinetic studies, the SMX and TMP concentrations in water were measured after 6 different time intervals. Kinetic data were fitted to the pseudo first-order equation and BMG model (developed by Behnajady et al. (2007)), according to Eq. (6) and 7, respectively.

$$\frac{C}{C_0} = e^{-kt} \quad (6)$$

$$\frac{C}{C_0} = 1 - \left[\frac{t}{m + bt}\right] \quad (7)$$

where k is the pseudo-first order rate constant (min^{-1}), t is time (min), C is the concentration (μg L^{-1}) of each antibiotic at a given irradiation time, C_0 is the initial concentration, and m (min) and b are two constants related to the initial reaction rate and maximum oxidation capacity, respectively. Fittings to the described kinetic models were obtained by non-linear regression analysis using GraphPad Prism version 8.0.1.

2.5.4. Catalyst reuse

The reuse of the catalyst was studied during multiple cycles of adsorption and photo-Fenton process under the same conditions applied in the previous experiments, ultrapure water at pH 8 containing 200 μg L^{-1} of SMX and TMP, H_2O_2 (5 mM) and optimal amount conditions of PAC-Fe catalyst. After each cycle, the catalyst was filtered, dried at 50 °C for 12 h, and reused in another cycle under the same conditions, without any regeneration step. The performance of the reused material was evaluated by comparing the percentage of antibiotics' removal (adsorption and photo-Fenton) after each cycle of 20 min.

2.5.5. Identification of transformation products and toxicity assessment

To allow for the detection of the transformation products generated during the photo-Fenton process, experiments were performed by using individual antibiotic solutions, changing the initial antibiotic concentration from 200 μg L^{-1} to 10 mg L^{-1} and the irradiation time to 120 min. Although the antibiotic concentration increased, the catalyst amount and H_2O_2 conditions were maintained as before. After conducting a preliminary analysis of the samples collected at different intervals over 120 min, the samples collected after 30 min were selected for transformation products analysis. The time was chosen considering the time at which a larger number of transformation products could be clearly identified in the chromatogram. The samples were filtered through a 0.22 μm filter previously to the analysis.

The transformation products of SMX and TMP were identified by ultra-high-performance liquid chromatography (UHPLC), using Ultimate 3000 equipment (Dionex Co., San Jose, CA, USA), equipped with a diode array detector (DAD) and coupled with a Thermo LTQ XL mass spectrometer (Thermo Scientific, San Jose, CA, USA) and an electrospray ionization interface (ESI). The elution was carried out with a mobile phase of 82:18 (*v/v*) 0.1 % formic acid: methanol at a flow rate of 0.15 mL min^{-1}. The injection volume was 10 μL, and detection was monitored at 270 nm. The column was Hypersil Gold C18 with 100 mm × 2.1 mm i.d. and 1.9 μm particle size. The instrument was operated in the positive-ion mode and with the ESI needle voltage set at 5 kV and an ESI capillary temperature of 275 °C. The full scan covered the mass range from *m/z* 110 to 2000. The data was processed using Thermo Xcalibur software, version 2.2.

The toxicity of the transformation products of SMX and TMP identified in the reaction medium to aquatic organisms was predicted using the Ecological Structure Activity Relationships (ECOSAR 2.2) software based on LC_{50} (50 % lethal concentration), EC_{50} (50 % effect concentration), and chronic toxicity (ChV).

3. Results and discussion

3.1. PAC-Fe characterization

XRD analysis results allow for assessing the existence of magnetic iron oxide within PAC-Fe (Fig 1). The diffraction patterns depicted in Fig. 1A illustrate the presence of peaks associated with both magnetite and maghemite oxides (observed at 2θ angles of 30.3, 53.3, 43.5, and 53.9 degrees), being challenging to definitively discern whether there is the presence of a single oxide or a coexistence of both types, as previously reported (Pereira et al., 2023). Yet, both magnetite and maghemite will confer magnetic properties to PAC-Fe, which are assessed below (see Table 1).

As presented in Fig. 1B, the PAC-Fe consistently displayed a negative surface charge over a wide pH range. Notably, some studies have indicated the likelihood of these pronounced negative charge values stemming from the formation of Fe–O–C bonds, which coexist with the presence of hydroxyl (OH) groups on the material's surface (Li et al., 2021; Zhu et al., 2020).

The surface images of the PAC-Fe before use reveal the presence of Fe as small spheres deposited onto the carbon surface (Fig. 2). Following one and three applications of PAC, it is possible to observe that the surface morphology of the material was maintained even after reuse. These results indicate the stability of the material, suggesting an effective deposition of iron onto its surface.

The determination of the surface chemical composition of PAC-Fe before and after its application in the photo-Fenton process was conducted through XPS. The atomic relative percentage (Table S1) in the surface layer (<5 nm), was extracted from high-resolution spectra (Fig. 3).

The survey spectra show the presence of four main peaks, assigned to C 1*s*, O 1*s*, N 1*s*, and Fe 2*p* and the presence of small peaks attributed to Si, S, Al, and Cl, evidencing trace amounts of these elements that might result from the reagents used in the synthesis (Fig. S1). The proposed assignment for each peak, along with their relative percentages, are detailed in Table S2. An analysis of the relative atomic abundance on the surface of the PAC-Fe using XPS data showed 76.8 % of carbon, 19.6 % of oxygen, 1.2 % of nitrogen and 2.4 % of iron.

For the C 1*s* spectra, the carbon binding energies are typical of aromatic carbon containing oxygenated groups. The main component at 284.5 eV is associated with aromatic groups (C—C sp^2) with

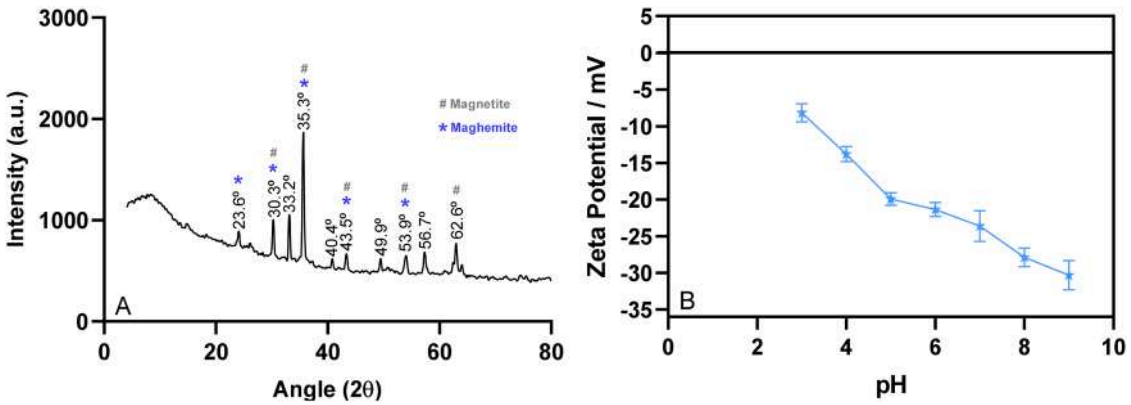

Fig. 1. (A) XRD patterns of PAC-Fe and (B) zeta potential of PAC-Fe as a function of pH.

Table 1
Specific surface area, pore morphology and vibrating sample magnetometer analysis for PAC-Fe.

Parameter	Measured value
Specific surface area ($m^2\ g^{-1}$)	41
Total pore volume ($cm^3\ g^{-1}$)	0.12
Total micropore volume ($cm^3\ g^{-1}$)[a]	0.02
Average micropore width (nm)[a]	1.95
Average pore diameter (nm)	5.87
Vibrating sample magnetometer analysis (emu g^{-1})	21.14

[a] Determined by Dubinin-Radushkevich equation (Marsh and Rand, 1970).

hydrocarbon contamination (C—H) at 284.8 eV. Oxygenated groups of alcohol and ether (C—O), carbonyl (*C*=*O*), and carboxyl (O—*C*=*O*) appear at 286.2 eV, 287.5 eV, and 289.3 eV, respectively. At higher binding energies (290.6 and 293.0 eV), satellites from the aromatic phase related to π-π* transitions are observed (Velo-Gala et al., 2014). The O 1*s* spectra are very similar for all samples, indicating that the main contributions come from O-Fe, O-Al groups at 530.2 eV, O—C, O-Si at 532.3 eV, and O—*C*=*O* groups at 533.4 eV, corroborated in the C 1*s* spectra, from the carbon matrix. The peak at 531.1 eV can be associated with the surface groups of -OH, *O*=*C* and Fe-OH (Zeng and Kan, 2022; Zhu et al., 2020). Regarding the deconvoluted N 1*s*, in addition to N—C (400.3 eV) and N—O (401.8 eV) groups, pyridine rings (398.4 eV) are also observed (Spessato et al., 2020), yet N functional groups were found in very small amounts in comparison to O functionalities. For all samples, the spin-orbit component $2p_{3/2}$ of the Fe 2*p* spectrum indicates that the predominant phase is Fe_2O_3 (710.5 eV), with a small contribution from FeOOH (712.5 eV) (de Jesus et al., 2022;de Jesus et al., 2023). All peaks are attributed to trivalent Fe (Zhu et al., 2020), with no indication of the presence of divalent Fe phase.

Although the XRD results revealed peaks which can be attributed to both magnetite and maghemite oxides (Fig. 1A), the absence of Fe(II) in the XPS data indicates that the iron oxide present on the surface of PAC-Fe is predominantly maghemite, considering that maghemite contains only Fe(III) whereas magnetite consists of a mixture of Fe(II) and Fe(III). The identification of a mixed oxide in the XRD results may be attributed to the inherent difficulty in distinguishing between these phases, given their spinel structure and nearly identical lattice parameters (Kim et al., 2012).

The results of the atomic percentage of elements (see Table sup) showed that there are no substantial changes in the PAC-Fe composition after application in the photo-Fenton process, even after 3 cycles of reuse. These results are consistent with SEM findings, where no morphological modifications in the material were observed, confirming its stability.

The results from textural characterization, as well as magnetic properties of the produced material are depicted in Table 1.

Regarding the S_{BET} and pore morphology, the results evidence that PAC-Fe is characterized by a mesoporous structure, with the micropore volume accounting for ~16 % of the total pore volume, and reasonable S_{BET} (41 $m^2\ g^{-1}$). The *Ms* points to 21.14 emu g^{-1} is higher than the majority of magnetic activated carbons reported in literature (Rocha et al., 2020), which leads to a decrease of S_{BET} due to the high load of Fe particles onto the PAC surface. These particles can cover the carbon surface, obstructing the interconnected pores on the surface, which can result in a lower S_{BET} value (Spessato et al., 2020). The reproducibility of synthesis was evaluated by comparing the S_{BET} and VSM values of PAC-Fe from two different production batches. The S_{BET} of 37 $m^2\ g^{-1}$ and VSM 24 emu g^{-1} are similar to the ones presented in Table 1 for the first batch of the referred material, a clear indication of the reproducibility of the production procedure.

3.2. Heterogeneous solar photo-Fenton experiments

3.2.1. Selection of PAC-Fe amount

The selection of the PAC-Fe amount was based on the results of the SMX and TMP removal (%) and H_2O_2 consumption during the photo-Fenton process after 10 min of irradiation (Fig. 4).

Increasing the PAC-Fe amount from 0.10 g L^{-1} to 0.25 g L^{-1} results in a substantial increase in the removal of both SMX and TMP, from 32 ± 3 % and 55 ± 2 % to 84 ± 3 % and 77 ± 3 %, respectively. However, increasing the amount from 0.25 g L^{-1} to 0.50 g L^{-1} did not yield a noteworthy enhancement in the removal (%). Similarly, it is evident that H_2O_2 consumption displayed a more substantial increase (> 100 %) when the PAC-Fe amount changed from 0.10 to 0.25 g L^{-1}. Nevertheless, the rise in consumption was comparatively lower (< 40 %) when the amount varied from 0.25 g L^{-1} to 0.35 g L^{-1} and 0.50 g L^{-1}. Therefore, based on the presented results, 0.25 g L^{-1} was selected as the most appropriate amount, since the removal (%) of SMX and TMP already showed a significant increase at this condition and higher amounts did not result in a significantly higher removal efficiency. Furthermore, the H_2O_2 consumption was not significantly higher when increasing the PAC-Fe amount from 0.25 g L^{-1} to 0.50 g $^{-1}$, suggesting that a higher catalyst amount does not result in a proportional increase of $HO^{\bullet}$ generation through the reaction with H_2O_2. Therefore, opting for a higher PAC-Fe amount may result in unnecessary catalyst expenditure.

Flame atomic absorption spectrophotometry analysis of SMX and TPM solutions after the photo-Fenton process (for all the evaluated amounts of material) indicated that the concentration of iron in the solution remained below the LOD (0.09 mg L^{-1}) evidencing that no significant leaching of iron occurred. This points out the stability of the PAC-Fe, even when applied at higher amounts, supporting the occurrence of a heterogeneous photo-Fenton process without relevant contribution of the homogeneous Fenton process.

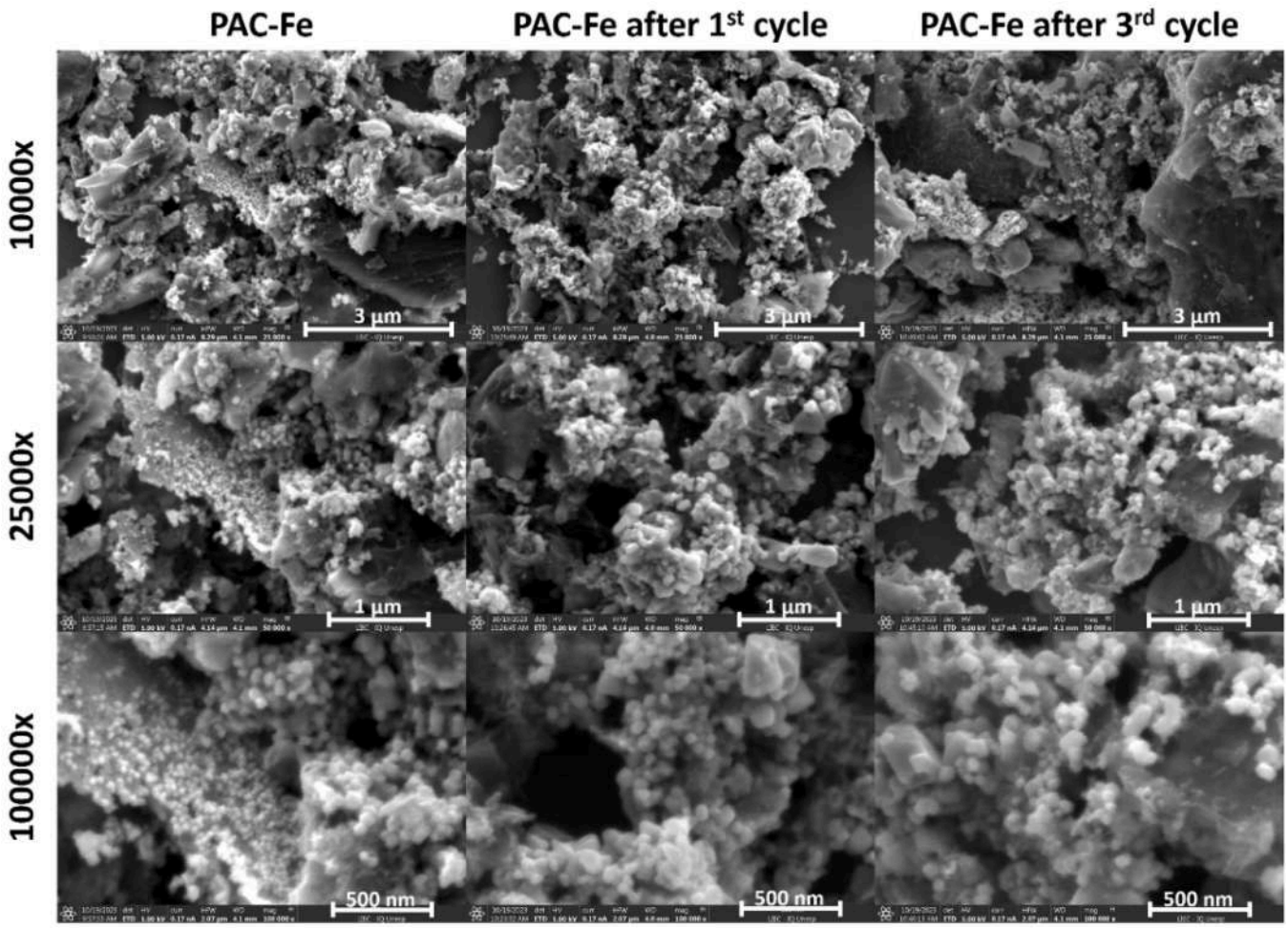

Fig. 2. SEM images of PAC-Fe before and after application on one and three consecutive photo-Fenton processes.

3.2.2. Evaluation of antibiotics removal through different processes

The removal of SMX and TMP can result from a combination of several processes. To determine the contribution of the different processes, the removal efficiency of SMX and TMP in six different conditions (photolysis (light), photo-assisted peroxidation (H_2O_2 + light), adsorption (PAC-Fe), photocatalysis (PAC-Fe + light), Fenton (PAC-Fe + H_2O_2) and photo-Fenton processes (PAC-Fe + H_2O_2 + light)) were compared (Fig. 5).

The removal (%) of SMX and TMP *via* photolysis was only 4 ± 1 % and 9 ± 4 %, respectively, after 15 min of irradiation. However, the removal (%) significantly improved in the presence of H_2O_2+light, resulting in 38 ± 1 % and 44 ± 1 % for SMX and TMP, respectively, which indicates that the presence of H_2O_2 substantially improves the degradation of antibiotics.

Removal due to adsorption onto PAC-Fe achieved 67 ± 2 % and 45 ± 3 % for SMX and TMP, respectively. Analyzing the pK_a and the corresponding speciation of each pharmaceutical (see Table S3 and Fig. S2) at the working pH 8.0, it can be stated that SMX is present in its anionic form, while TMP is mainly in the neutral form. In this scenario, if the electrostatic interactions were the ones ruling the adsorption process and considering that the surface of PAC-Fe is predominantly negative (see Fig. 1B, for zeta potential), it would be expected that PAC-Fe presented the highest removal (%) towards TMP. As highlighted by Li et al. (2023), the adsorption of hydrophilic compounds is not solely governed by electrostatic forces. Additional factors related to the material surface chemistry and molecular structure of the pharmaceutical can result in enhanced adsorption, such as hydrogen bonding and π-π interactions. The presence of hydroxyl and carboxyl groups on the PAC-Fe surface may indeed facilitate adsorption via hydrogen bonding, while the aromatic rings in both structures can promote π-π interactions with the highly aromatic structure of PAC-Fe. A closer analysis to other physical-chemical properties of the pharmaceuticals (Table S3) indicates that SMX has higher water solubility (S_w) and lower octanol-water partition coefficient (log K_{ow}) than TMP, revealing its higher tendency to remain in the aqueous phase in comparison to TMP. If only these physical-chemical properties would control the adsorption process, TMP is expected to adsorb more than SMX. Considering both SMX and TMP are hydrophilic compounds and given that electrostatic forces are expected to have minimal contribution to their adsorption on PAC-Fe, it is plausible to suggest that hydrogen bonding may exert a more pronounced influence in this process. Recently, Li et al. (2022) elucidated that the predominant mechanism of SMX adsorption onto biochar was primarily related to pore filling and π-π interactions under acidic conditions. However, under alkaline conditions with a pH above 8, where both SMX and applied biochar exhibited negative charges, contrary to the expectation of repulsion, adsorption mainly occurred due to pore filling and hydrogen bond formation.

TMP adsorption may also occur due to the formation of hydrogen bonds, considering the presence of methoxy groups on the benzene ring and two amine groups on the pyrimidine ring in its structure, which can serve as potential acceptors for these bonds. Additionally, the adsorption mechanism of this antibiotic can also occur through interactions between the aromatic phase of biochar and the trimethoxy benzene ring via π-π interactions (Le et al., 2024). In addition to the interactions of each antibiotic with biochar, competitive effects between antibiotics in solution can occur. As evidenced by Sousa et al. (2023), the presence of

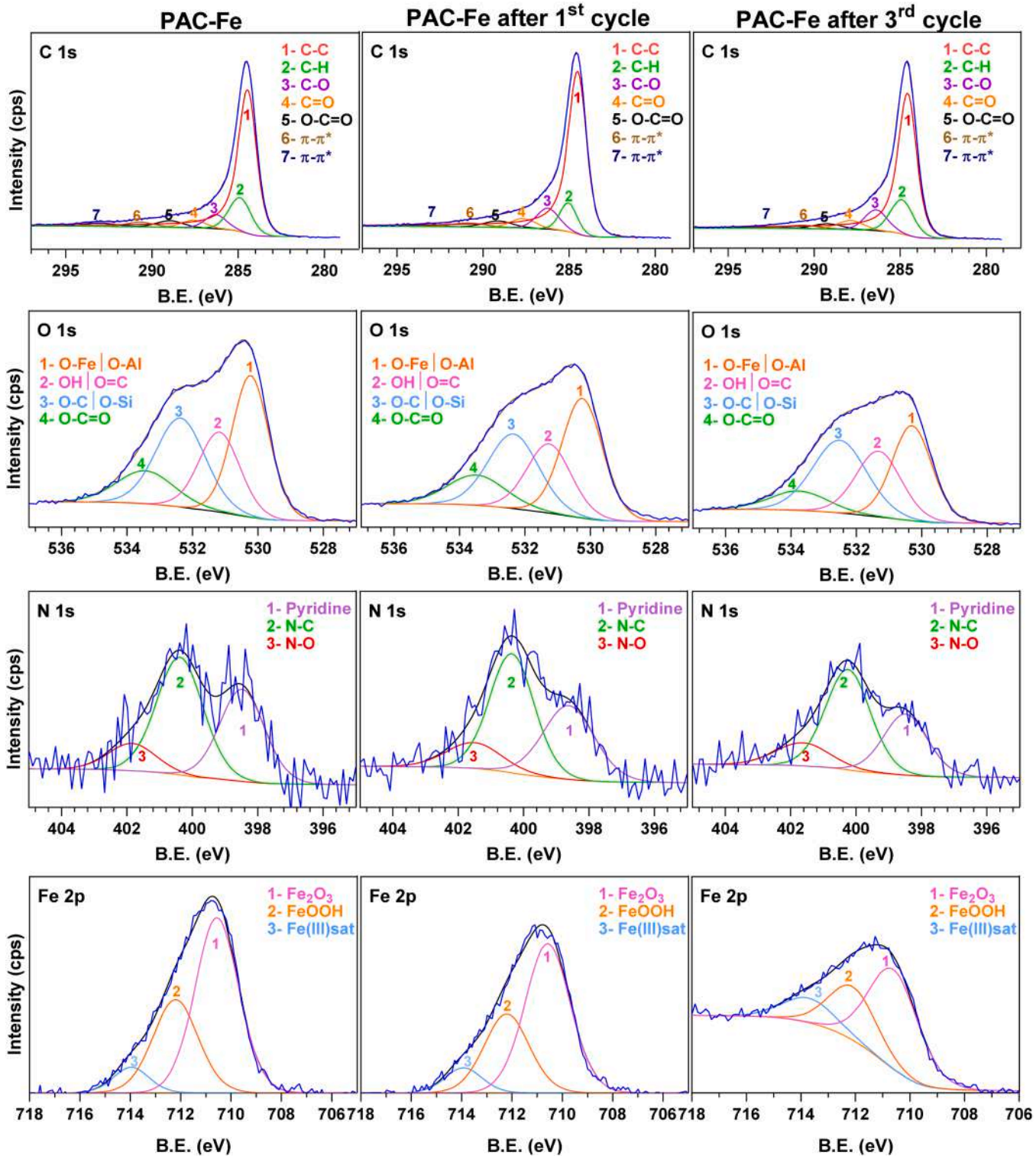

Fig. 3. C 1*s*, O 1*s*, N 1*s* and, Fe 2*p* XPS spectra of PAC-Fe before and after one and three consecutive photo-Fenton processes.

SMX can unfavorably affect TMP adsorption, and vice versa. Therefore, predicting the behavior of antibiotics by adsorption in a mixture becomes challenging.

When comparing adsorption (PAC-Fe) and photocatalysis (PAC-Fe + light), the removal (%) by each of these processes was very similar for both SMX and TMP. This suggests that adsorption was the main process occurring in solution and that irradiation did not significantly increase the removal of these pharmaceuticals, evidencing no remarkable photocatalytic activity of PAC-Fe.

Comparing the heterogeneous process, Fenton (PAC-Fe + H_2O_2) and photo-Fenton (PAC-Fe + H_2O_2 + light), the removal (%) due to the Fenton process was 85 ± 1 % and 85 ± 3 % for SMX and TMP, respectively, while for the photo-Fenton process was 95 ± 1 % for SMX and 93 ± 5 % for TMP. The results presented suggest that the photo-Fenton and Fenton heterogeneous processes were the most effective in removing the compounds under study, followed by adsorption. Overall, adsorption

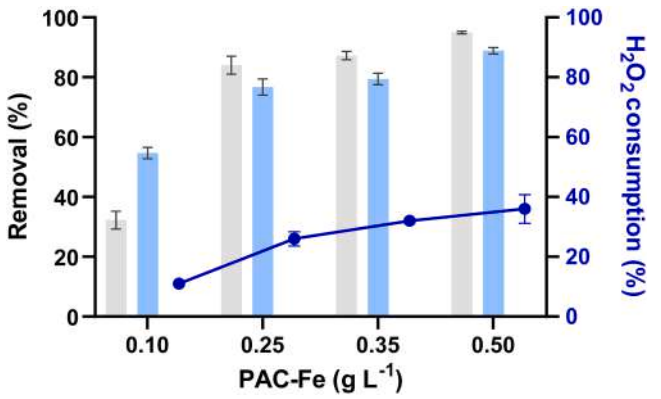

Fig. 4. Removal of SMX ( ) and TMP ( ), after 10 min of irradiation with different PAC-Fe amounts, and H_2O_2 consumption (●). Conditions: SMX and TMP initial concentration 200 μg L^{-1}, 5 mM H_2O_2 and pH 8.0. Note: Error bars stand for standard deviation, n = 3.

can serve as the initial step, whereby the catalyst adsorbs antibiotics and H_2O_2 onto its surface. On the PAC-Fe surface, iron ions can interact with H_2O_2, leading to the production of $HO^{\bullet}$, which then reacts with SMX and TMP (Seidmohammadi et al., 2021). It is important to highlight that since PAC-Fe demonstrated stability during the application, with no apparent changes in composition as indicated by the XPS analyses, and no iron leaching to the solution, the contribution of the homogeneous Fenton process to degradation was considered irrelevant.

3.2.3. *Kinetic of antibiotics removal from aqueous samples*

Considering the results obtained in Section 3.2.2, kinetic studies were carried out to evaluate the influence of all the processes in the removal of antibiotics from ultrapure water under pH 8, over a duration of 20 min. For comparison purposes, the contribution of all processes (photolysis, photo-assisted peroxidation, adsorption, photocatalysis, Fenton and photo-Fenton processes) in the removal kinetics is shown in Fig. 6.

The results confirmed that photolysis and photocatalysis processes do not play a significant role in the removal of antibiotics, with photo-assisted peroxidation, adsorption, Fenton, and photo-Fenton processes being the most relevant, as mentioned earlier in Section 3.2.2.

Adsorption was found to be a relevant process in the removal of SMX and TMP by PAC-Fe, as a quick decrease of their concentrations was observed (Fig. 6), evidencing the rapid uptake of these antibiotics from aqueous media. However, the adsorption equilibrium was achieved after the 20 min experiment, resulting in a final removal of 68 ± 5 % for SMX and 46 ± 2 % for TMP, which indicates that higher removal of SMX and TMP cannot be achieved at these conditions. The removal due to the Fenton process also reached equilibrium, while complete removal, with concentrations <LOD, was only achieved with the photo-Fenton process, revealing that the use of PAC-Fe in heterogeneous photo-Fenton processes is an effective strategy to enhance the removal of SMX and TMP from water.

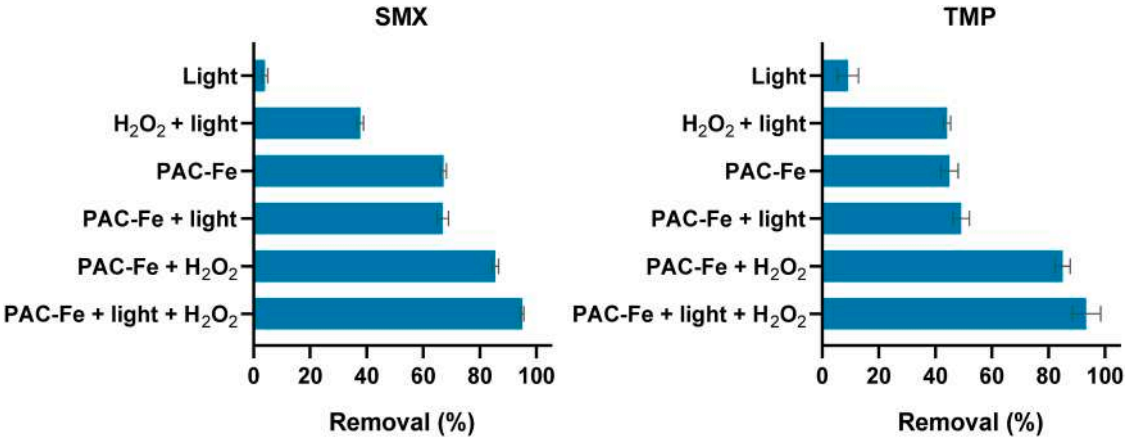

Fig. 5. Comparison of removal efficiency of SMX and TMP after 15 min, using different processes. Conditions: SMX and TMP initial concentration 200 μg L^{-1}, PAC-Fe 0.25 g L^{-1}, 5 mM H_2O_2 and pH 8.0. Note: Error bars stand for standard deviation, n = 3.

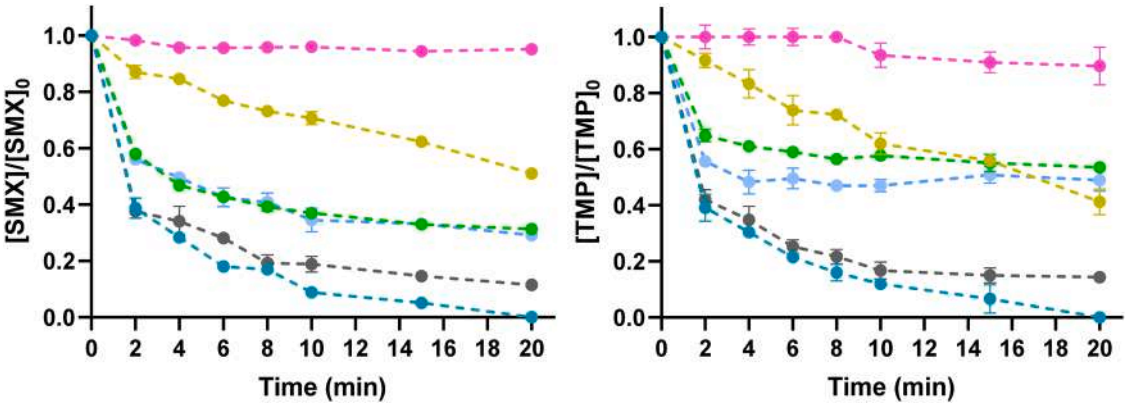

Fig. 6. Removal of SMX and TMP under photolysis (●), photo-assisted peroxidation (●), adsorption (●), photocatalysis (●), Fenton (●) and photo-Fenton processes (●). Conditions: SMX and TMP 200 μg L^{-1}, PAC-Fe 0.25 g L^{-1}, H_2O_2 5 mM and pH 8.0. Note: Error bars stand for standard deviation, n = 3. The dashed lines were included solely to facilitate the visualization and tracking of the evolution of each process. They do not hold any statistical or interpretative significance.

Based on these results, two kinetic models were applied to study the two processes that contribute the most to the removal of antibiotics. The graphical representation (C/C_0 *vs* time (min)) for SMX and TMP by both Fenton and photo-Fenton processes by fitting the experimental data to the pseudo first-order and BMG kinetic models are presented in Fig. 7 and Table 2 shows the kinetic parameters obtained (as described in Section 2.5.3).

The fittings in Fig. 7 and the R^2 in Table 2 for both Fenton and photo-Fenton processes evidenced that the BMG kinetic model outperformed the pseudo first-order kinetic model in describing the experimental data accurately. The BMG model achieved higher R^2 values, ranging from 0.988 to 0.995, while the pseudo first-order models consistently obtained R^2 values below 0.95. The better fit of the BMG model compared to pseudo first-order kinetics indicates that the removal process is influenced by multiple and simultaneous mechanisms. This has important implications for scaling up, as it suggests that the process efficiency may depend on multiple factors such as contaminant concentration, catalyst dosage, and mixing conditions, which is crucial for optimizing operational parameters in large-scale applications.

The empirical model BMG, developed by Behnajady et al. (2007), aimed to study the kinetics of the Fenton process in dye degradation, and considered two distinct stages in the Fenton reaction: an initial rapid phase and a subsequent slower one. In the classical Fenton reaction, the fast initial phase is mainly a result of the interaction between Fe^{2+} and H_2O_2, while the slower phase is attributed to the accumulation of Fe^{3+} and the limited regeneration of Fe^{2+} through H_2O_2 (Jiang et al., 2022). Therefore, representing this two-stage process based solely on pseudo first-order reaction kinetics becomes inadequate. In this sense, the BMG model has been applied in studies to assess the degradation kinetics of dyes (Li and Cheng, 2021) and organic solvents (Behrouzeh et al., 2020) through the Fenton process. Moreover, it has been employed in a system similar to the one studied in this work, where biochar modified with iron was used for SMX degradation in water, combining adsorption and heterogeneous Fenton processes (Liu et al., 2023). These applications have demonstrated the adequacy of BMG model in describing reactions with a faster initial onset and a subsequent slower step.

For the BMG model, a higher $1/m$ value indicates a faster initial degradation rate. When comparing Fenton and photo-Fenton processes, the values of $1/m$ for both antibiotics were similar. However, upon analyzing the maximum degradation capacity ($1/b$) of the BMG model for SMX and TMP, the $1/b$ values are higher in the photo-Fenton process than in Fenton process. Overall, the results demonstrate that both processes exhibited rapid initial degradation, as indicated by similar values of $1/m$. However, in the Fenton process, the degradation rate decelerated over time, resulting in a constant decay of concentration as seen in Fig. 7, without reaching complete degradation (concentrations < LOD), corroborated by the smaller value of $1/b$. On the contrary, in the photo-Fenton process, degradation persisted and achieved total removal after 20 min, indicating a greater degradation capacity of this process if compared to Fenton, represented by the higher value of $1/b$. These differences between Fenton and photo-Fenton processes can be attributed to the presence of light, suggesting that solar radiation increases the degradation performance of the materials. As highlighted by Bokare and Choi (2014), catalysts impregnated predominantly with Fe(III) require light to enhance the reductive generation of Fe(II), since the reaction between Fe(III) and H_2O_2 is notably slower if compared to the classical Fenton reaction (Fe(II) and H_2O_2) (Eq. (1) and 2). This deceleration can pose a significant obstacle to the effective formation of $HO^{\bullet}$, thereby compromising the degradation process of the target compounds.

Table 2
Fitting parameters (pseudo first-order rate constants (k), BMG model initial degradation rate ($1/m$) and the maximum degradation capacity ($1/b$), and coeficient of determination (R^2)) obtained for Fenton and photo-Fenton processes for SMX and TMP.

	First-order		BMG model		
	k (min^{-1})	R^2	$1/m$ (min^{-1})	$1/b$	R^2
SMX					
Fenton	0.23 ± 0.05	0.854	0.686 ± 0.001	0.89 ± 0.03	0.988
photo-Fenton	0.31 ± 0.04	0.951	0.88 ± 0.03	1.02 ± 0.03	0.995
TMP					
Fenton	0.22 ± 0.05	0.889	0.7 ± 0.1	0.92 ± 0.02	0.995
photo-Fenton	0.29 ± 0.05	0.940	0.7 ± 0.1	1.00 ± 0.03	0.995

Considering that XPS results (see Fig. 3, Section 3.1) revealed that the catalyst surface is predominantly composed of Fe(III), it becomes evident that the irradiation can directly impact the system's performance by iron reduction. Furthermore, irradiation also contributes to the generation of the $HO^{\bullet}$ through photo-assisted peroxidation which, as previously demonstrated, also plays a role in the degradation of the antibiotics.

The effectiveness of PAC-Fe in removing SMX and TMP from water using the Fenton or photo-Fenton processes was compared with other catalysts (Table 3). PAC-Fe is equally or more effective than other catalysts reported in the literature, especially when considering that the same or superior degradation efficiencies were achieved in a shorter irradiation time. For SMX, PAC-Fe achieved 100 % of removal at pH 8, within a brief irradiation period of 20 min under simulated solar radiation. Other studies have also reported SMX removal of up to 100 % but using catalysts at non-adjusted pH (considering that the studies were carried out in ultrapure water, the working pH is considered to be ~5–6) (de Jesus et al., 2022; Nawaz et al., 2020) or at unrealistic pH values of ≤3 (Zeng and Kan, 2022; Zárate-Guzmán et al., 2020; Lima et al., 2017; Singh et al., 2022) (specially, when considering an environmentally relevant application), except the study reported by Gao et al. (2018),

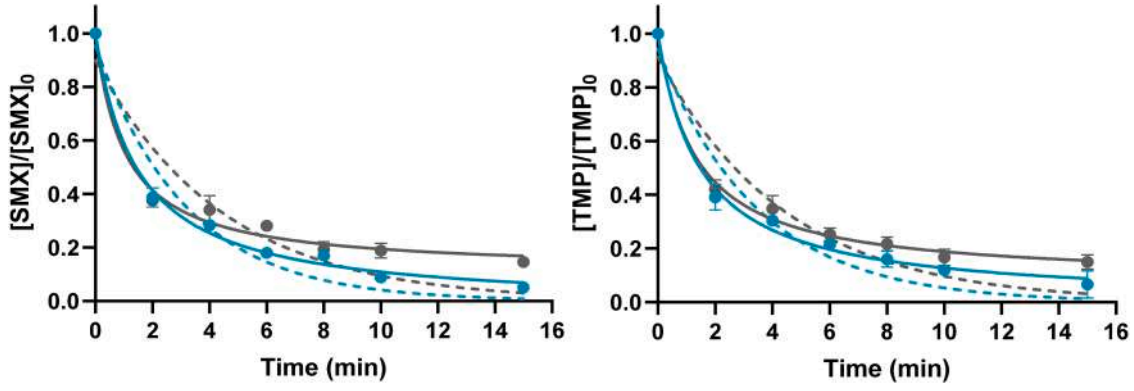

Fig. 7. Degradation kinetics obtained for SMX and TMP for Fenton (●) and photo-Fenton (●) processes. Fittings to pseudo first-order model (dashed line) and BMG model (full line) are represented together with the corresponding experimental results. Conditions: SMX and TMP 200 μg L^{-1}, PAC-Fe 0.25 g L^{-1}, H_2O_2 5 mM and pH 8.0. Note: Error bars stand for standard deviation, n = 3.

Table 3
Comparison of catalysts applied in photo-Fenton and Fenton processes for the removal of SMX and TMP from water.

Antibiotic	Process	Catalyst	Experimental conditions (Antibiotic initial concentration; material amount; H_2O_2 concentration; pH)	Irradiation	Time (min)	Efficiency (%)	Reference
SMX	Photo-Fenton	$NiFeO_4$	5000 μg L^{-1}; 0.025 g L^{-1}; 9.8 mM; pH not adjusted	UV-A	120	100	(Nawaz et al., 2020)
		$NiFeO_4$	5000 μg L^{-1}; 0.025 g L^{-1}; 9.8 mM; pH not adjusted	Visible	120	100	(Nawaz et al., 2020)
		$CuFe_2O_4$	10,000 μg L^{-1}; 0.2 g L^{-1}; 10 mM; pH 6.73	Visible	120	100	(Gao et al., 2018)
		PA-CNC	50,000 μg L^{-1}; 0.5 g L^{-1}; 8.8 mM; pH 2.5	Visible	60	77.8	(Singh et al., 2022)
		PAC-Fe	200 μg L^{-1}; 0.25 g L^{-1}; 5.0 mM; pH 8.0	Simulated Solar radiation	20	100	This work
	Fenton	$FeCl_3$-AC	100,000 μg L^{-1}; 0.1 g L^{-1}; 1.5 mM; pH 3.0	–	720	98.3	(Zeng and Kan, 2022)
		Fe@MesoC	20,000 μg L^{-1}; 0.2 g L^{-1}; 3.0 mM; pH 4.0	–	120	100	(Tang and Wang, 2018)
		Carbon-Fe	20,000 μg L^{-1}; 0.5 g L^{-1}; 2.5 mM; pH 3.0	–	120	98	(Zárate-Guzmán et al., 2020)
		PAC-Fe	200 μg L^{-1}; 0.25 g L^{-1}; 5.0 mM; pH 8.0	–	20	88.5	This work
TMP	Photo-Fenton	Fe_2O_3-TiO_2	10,000 μg L^{-1}; -; 2.5 mM; pH 2.5	Simulated Solar radiation	240	66	(Lima et al., 2017)
		$[Cu_{0.5}Fe_{0.5}][Fe_2]O_4$–Clay	300 μg L^{-1}; 0.5 g L^{-1}; 10 mM; pH not adjusted	Natural solar radiation	180	100	(de Jesus et al., 2022)
		PAC-Fe	200 μg L^{-1}; 0.25 g L^{-1}; 5 mM; pH 8.0	Simulated Solar radiation	20	100	This work
	Fenton	$[Fe][Fe_2]O_4$–Clay	300 μg L^{-1}; 0.5 g L^{-1}; 10 mM; pH not adjusted	–	180	66	(de Jesus et al., 2022)
		$[Cu_{0.5}Fe_{0.5}][Fe_2]O_4$–Clay	300 μg L^{-1}; 0.5 g L^{-1}; 10 mM; pH not adjusted	–	180	58	(de Jesus et al., 2022)
		PAC-Fe	200 μg L^{-1}; 0.25 g L^{-1}; 5 mM; pH 8.0	–	20	85.7	This work

that applied $CuFe_2O_4$ at pH 6.7. However, a very high antibiotic initial concentration (10,000 μg L^{-1}) was employed, as well as a higher concentration of H_2O_2 (10 mM), and a longer irradiation time of 120 min, making it less feasible for real-world applications.

Similarly, for TMP removal, 100 % efficiency was also achieved at circumneutral pH, while all the studies presented in Table 3 were operated under non-relevant matrix conditions (non-adjusted pH or pH $\leq$ 2.5), reporting removal efficiencies between 58 % and 100 %. Based on these findings, it can be concluded that PAC-Fe demonstrated effective performance in the removal of SMX and TMP at an environmentally relevant pH, suggesting its suitability for neutral to moderately alkaline conditions. Future studies will assess the application of PAC-Fe in real samples to evaluate the impact of the matrix on the catalyst activity and the efficiency of the photo-Fenton process. Matrix components, both organic and inorganic, such as carbonate and chloride ions, can directly influence the reaction by acting as scavengers of $HO^{\bullet}$. Therefore, it is essential to study the process performance in more complex matrices to ensure its effectiveness under real conditions.

3.2.3. *Catalyst reuse*

The multiple reuse of a catalyst is an important feature for practical applications (Liu et al., 2012; Chai et al., 2016). Fig. 8 depicts the results from the PAC-Fe reuse up to five cycles, according with experimental conditions described in Section 2.5.4. The graphical representation shows the impact of PAC-Fe reuse cycles in SMX and TMP removal with emphasis on the evaluation of two different processes, namely photo-Fenton and adsorption.

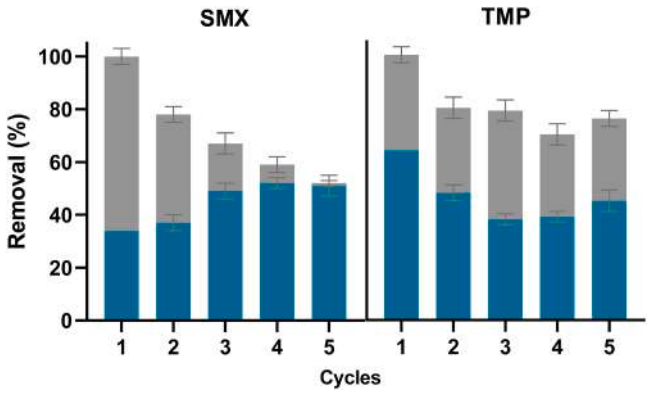

Fig. 8. Reuse of PAC-Fe for the removal of SMX and TMP by photo-Fenton (▬) and adsorption (▬) process over 5 cycles of 20 min each. Conditions: SMX and TMP 200 μg L^{-1}, H_2O_2 5 mM, PAC-Fe 0.25 g L^{-1}, and pH 8.0. Note: Error bars stand for standard deviation, n = 3.

As shown in Fig. 8, after going through every cycle, the removal percentage decreased, and after five cycles the overall SMX removal gradually decreased from 100 % (cycle 1) to 52 ± 4 % (cycle 5). It is important to highlight that the gradual decrease in the overall SMX removal after five cycles of reuse of PAC-Fe is related to the adsorptive saturation of the material, due to the decrease in the availability of active adsorption sites in the PAC-Fe surface, as demonstrated by the decreasing contribution of adsorption for the global removal process. As evidenced, adsorption was the main process occurring for SMX during cycles 1 and 2. However, the contribution of adsorption gradually decreased over subsequent cycles and from the third to the last cycle, the photo-Fenton process became the main removal mechanism. If the efficiency of PAC-Fe is evaluated only considering its activity in photo-Fenton process catalytic activity, it is noteworthy that no loss of performance was observed, pointing to a regeneration of the catalyst surface at each addition of H_2O_2.

In the case of TMP, the removal is constant after the second cycle, decreasing only 4 % between cycle 2 and 5. The contribution of adsorption and photo-Fenton processes is balanced during the reuse cycles, with both processes influencing the overall removal percentage. The removal of TMP by the photo-Fenton process also remained stable after cycle 2, demonstrating that the catalyst maintains its activity. This corroborates the idea that PAC-Fe does not lose its catalytic activity for application in the photo-Fenton process. These results are consistent with SEM and XPS analyses, which did not show significant changes in the morphology and composition of the material after use. Additionally, atomic absorption analysis did not detect the presence of Fe in the solution, suggesting that there was no measurable loss of Fe from the catalyst surface during the process. Therefore, PAC-Fe can be considered a stable catalyst applicable in multiple cycles of the heterogeneous photo-Fenton process.

3.3.4. *Identification of transformation products and toxicity assessment*

To identify the transformation products of SMX and TMP resulting from the photo-Fenton process, the MS spectra of the samples obtained after photo-Fenton process were compared with the spectra of the SMX and TMP standard solutions before the process. The molecular ions [M +

$H]^+$ of the potential transformation products were identified and tentative assignments of the molecular formula and structures of the products were made based on the fragmentation patterns observed in the MS^2 spectra (see detailed data in Table S4). This analysis enabled the identification of specific products formed during the photo-Fenton process and provided important insights into the degradation mechanism of the antibiotics SMX and TMP.

Eight transformation products of SMX were identified arising from distinct reaction pathways (Fig. 9). To the best of our knowledge, one of these intermediate products (SMX6 *m/z* 257) have not been previously reported. Pathway I involves the di-hydroxylation of the isoxazole ring, which can result from the epoxidation of the C—C double bond, followed by epoxide ring opening and formation of the diol. This pathway leads to the formation of SMX1 (*m/z* 288) (Tang et al., 2023; Li et al., 2023; Gómez-Ramos et al., 2011). Pathway II is an electrophilic substitution by the $HO^{\bullet}$ group that occurs in the aromatic ring, resulting in SMX2 (*m/z* 270), which is in line with previous studies (Gómez-Ramos et al., 2011; Gao et al., 2020; Huang and Yang, 2021; Wang et al., 2011; Wang et al., 2022). During the photodegradation of SMX, a rearrangement of the isoxazole ring (pathway III) was also observed, resulting in SMX3 (*m/z* 254), a well-known photoisomer. This photoproduct has previously been detected as a direct result of SMX photolysis (Trovó et al., 2009; Voigt et al., 2017; Yang et al., 2017), indicating that photolysis of SMX also occurs during the photo-Fenton process. This product has the same *m/z* value as SMX itself and a lower retention time on a reversed-phase HPLC column, as is the case in our study. As described by Wang et al. (2022), pathway IV demonstrates a selective oxidation of the amino group in the benzene ring to generate SMX4 (*m/z* 268). According to theoretical studies, the nitrogen from the aniline amino group seems to be the most reactive nitrogen of the SMX molecule (Liu et al., 2023; Li et al., 2024). Another route (V) involves the substitution of the amino group through the attack of the $HO^{\bullet}$ radical on the aniline ring (Wang et al., 2011; Gmurek et al., 2015). This leads to the release of NH_4^+ by breaking the C—N bond, and the formation of compound SMX5 (*m/z* 271) after hydroxylation of the benzene ring. Pathway VI is proposed to generate SMX6 (*m/z* 257), which, to the best of our knowledge, has not been previously reported. SMX6 can be generated by losing the NH_4^+ group on the aniline aromatic ring (after breaking the C—N bond, similarly to what occurs during the formation of SMX5) combined with the hydroxylation of the isoxazole ring. This hypothesis is reinforced by the absence of both the fragments corresponding to daughter ions with *m/z* 99 and *m/z* 156 in the MS^2 spectrum obtained for *m/z* 257 parent ion, meaning that both SMX rings (aniline and isoxazole) were modified. On the other hand, SMX7 (*m/z* 304) can result from the hydroxylation of the benzene ring coming from SMX1, or the same product can be formed by the di-hydroxylation of the isoxazole ring of SMX2. Although it was not possible to obtain the MS^2 spectra of SMX7, the formation of this product was suggested by the presence of the peak corresponding to *m/z* 304 in the MS spectrum (Fig. S3), aligned with the identification carried out by Stando et al. (2022). Additionally, the formation of SMX8 (*m/z* 302) can be considered an indication of the presence of SMX7, as SMX8 can be formed by the oxidation of SMX7 in the secondary hydroxyl group of the isoxazole ring (Pathway VII).

For TMP, fourteen transformation products were identified, formed through proposed distinct reaction pathways involving both the 3,4,5-trimethoxybenzene and the 2,4-diaminopyrimidine rings (Fig. 10). Similarly to SMX, the degradation of TMP involves hydroxylation of the molecule, extensively discussed in previous studies as the predominant transformation route due to the non-selectivity of $HO^{\bullet}$, which can attack both rings and the methylene bridge in TMP (Chen et al., 2024; Hasija

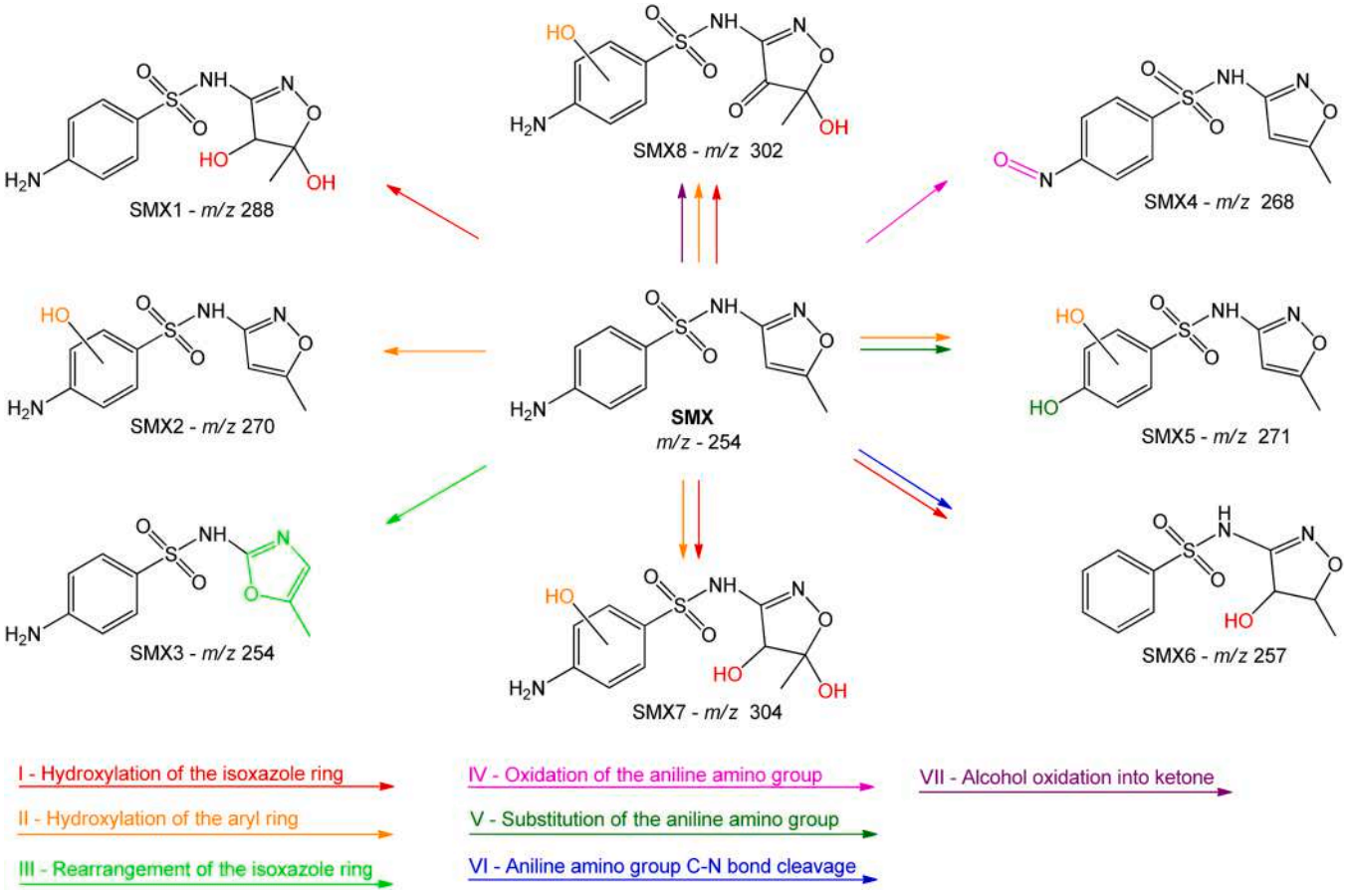

Fig. 9. Proposed degradation pathways of SMX by photo-Fenton using PAC-Fe as catalyst. Conditions: SMX 10 mg L^{-1}, H_2O_2 5 mM, PAC-Fe 0.25 g L^{-1}, pH 8.0. All *m/z* values correspond to $[M + H]^+$ molecular ions.

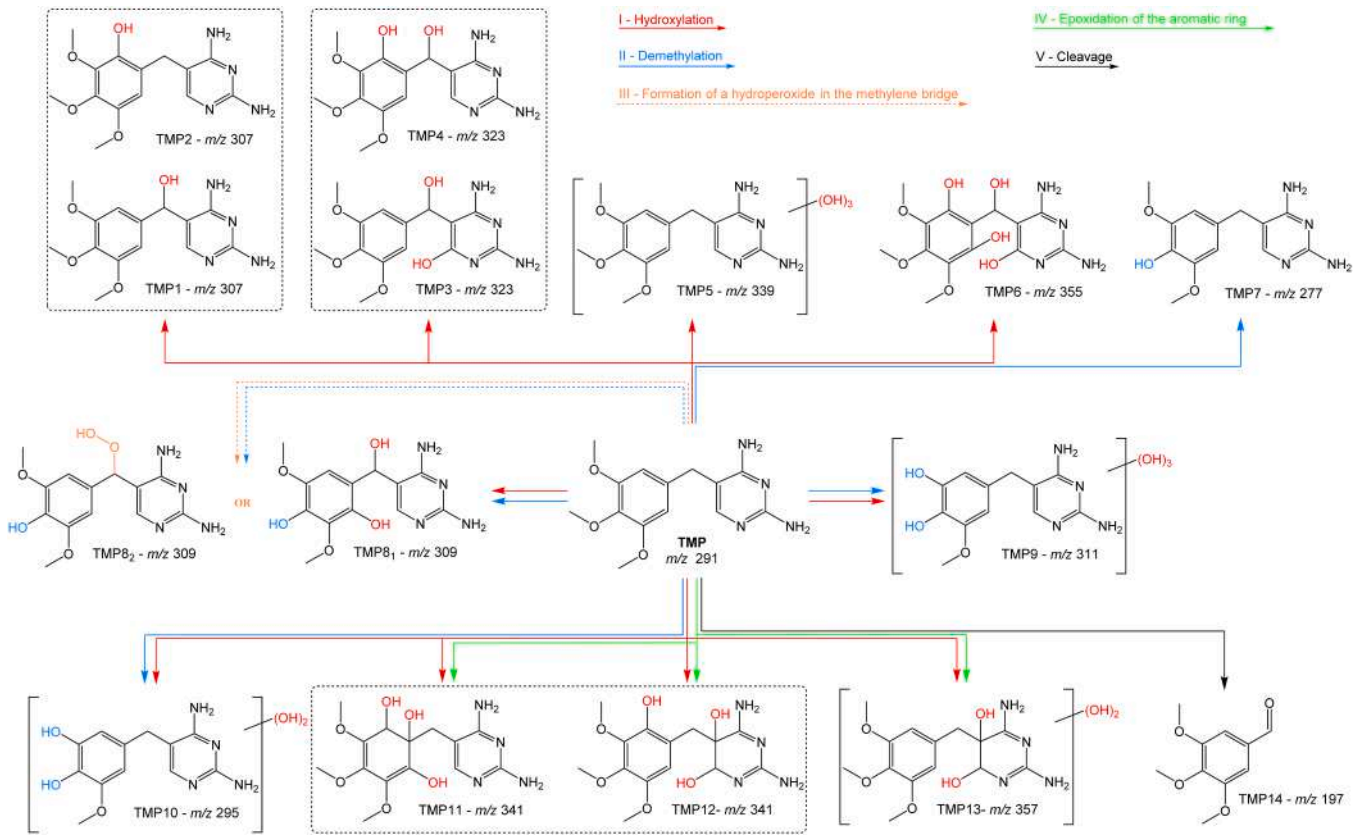

Fig. 10. Proposed degradation pathways of TMP by photo-Fenton using PAC-Fe as catalyst. Conditions: TMP 10 mg L^{-1}, H_2O_2 5 mM, PAC-Fe 0.25 g L^{-1}, pH 8.0. All *m/z* values correspond to $[M + H]^+$ molecular ions.

et al., 2022; Fan et al., 2021; Wei et al., 2024; Samy et al., 2020; Mo et al., 2024; Huang et al., 2024). So, the mono-hydroxylation products of TMP include TMP1 (*m/z* 307) and its positional isomer TMP2 (*m/z* 307), whereas TMP3 (*m/z* 323) results from di-hydroxylation of TMP, along with its isomer TMP4 (*m/z* 323). Moreover, TMP5 (*m/z* 339) corresponds to the insertion of three hydroxy groups and TMP6 (*m/z* 355) results from the tetra-hydroxylation of TMP (Cai and Hu, 2017; Sirtori et al., 2010; Wang and Wang, 2018; Zhang et al., 2020; Psutka et al., 2018). On the other hand, the demethylation of the initial TMP molecule yields TMP7 (*m/z* 277), since it was demonstrated, by density functional theory calculations, that the *C*−*O* bonds of the methoxy groups in the TMP molecule have the smallest Mulliken population value, indicating its easy fracture characteristic, leading mainly to the formation of TMP7 (Wei et al., 2024; Jewell et al., 2016). In this study, two hypothesis are proposed for TMP8 structure with *m/z* 309. The first is TMP8$_1$, resulting from the combination of hydroxylation and demethylation (Sirtori et al., 2010; Zhang et al., 2020), and TMP8$_2$, possibly generated by the formation of a hydroperoxide in the methylene bridge. As far as we know, this latter structure has not yet been reported in the literature. However, as it is consistent with the losses observed in the MS^2 profile of the precursor ion, it is also considered a potential structure for TMP8. The demethylation pathway, combined with the hydroxylation of TMP, may also lead to the formation of TMP9 (*m/z* 311), TMP10 (*m/z* 295), in agreement with previous findings (Sirtori et al., 2010; Zhang et al., 2020). In a different pathway, TMP can be epoxidized in the benzenic ring or pyrimidine ring and, by epoxide ring opening and formation of the corresponding diol followed by mono-hydroxylation, can lead to the formation of isomers TMP11 (*m/z* 341) and TMP12 (*m/z* 341). Furthermore, the hydroxylation of TMP12 can give rise to TMP13 (*m/z* 357). Lastly, the TMP molecule cleavage occurring at the methylene bridge results in the sole product called TMP14 (*m/z* 197). This product was initially identified by Sirtori et al. (2010) during the investigation of the products generated from the direct photolysis of TMP in surface waters.

Besides providing crucial insights into the degradation pathway of SMX and TMP, the investigation of the transformation products has yielded essential data concerning the efficiency of the PAC-Fe photo-Fenton process in removing such antibiotics. The chromatograms and spectra presented in Fig. S3 and Fig. S4 of the SM, depicting antibiotic profiles before and after the photo-Fenton process, reveal that after 120 min of reaction, no peaks were detected for both antibiotics and their transformation products. This fact decisively confirms the effectiveness of the catalyst, indicating that the photo-Fenton process successfully achieved the complete degradation of antibiotics and their intermediates. These results have significant implications, as complete antibiotic degradation is crucial for mitigating their adverse environmental impacts.

The toxicity assessment of SMX and TMP transformation products is essential to understand the environmental impact of these compounds. Data obtained using the ECOSAR software (Table S5) indicated a wide variability in toxicity. The transformation products SMX2, SMX5, SMX8, TMP2, TMP3, TMP7, and TMP8 presented low LC_{50} and EC_{50} values for daphnids and green algae, suggesting a high environmental risk. Additionally, transformation products containing phenol amine groups showed increased toxicity for different aquatic organisms, indicating that these chemical structures may enhance the ecotoxicological effects of these compounds. In contrast, TMP11 and TMP12 exhibited the highest LC_{50}, EC_{50}, and ChV values, indicating low toxicity.

Overall, the results highlight the importance of considering transformation products in the environmental risk assessment of antibiotics, as some may be more toxic than their parent compounds. However, it is important to emphasize that after 120 min of the photo-Fenton process applying PAC-Fe, UHPLC-MS analyses showed the complete removal of both SMX, TMP, and their transformation products, indicating that the

process is efficient enough to prevent environmental impacts by ensuring the complete removal of these compounds.

4. Final remarks

In the present study, a PAC-Fe composite was produced by loading magnetic iron oxides onto a waste-based PAC via one-step synthesis. The PAC-Fe was efficiently applied in the removal of SMX and TMP from ultrapure water by heterogeneous solar photo-Fenton. The elimination of both antibiotics was accomplished within a brief 20-min timeframe, under environmentally relevant pH conditions (pH 8). It is noteworthy that the removal of antibiotics by PAC-Fe is a complex process, which can occur through a combination of various mechanisms with adsorption, photo assisted peroxidation, Fenton and photo-Fenton processes working simultaneously. However, complete removal of both antibiotics was only achieved with the application of the photo-Fenton process under the tested conditions. The reuse studies have demonstrated that while the adsorptive capacity of PAC-Fe may decline over time, its catalytic activity is preserved across 5 consecutive cycles. The identification of the transformation products provided evidence that hydroxylation is the main degradation pathway for SMX and TMP. In this analysis a new product for SMX was observed and it was possible to verify the efficiency of the PAC-Fe, which was responsible for the complete removal of SMX, TMP (10 mg L^{-1}) and their respective photoproducts after 120 min.

These findings highlight the promising potential of employing the PAC-Fe material in photo-Fenton processes for the highly effective removal of SMX and TMP from aquatic environments, contributing with valuable insights into sustainable approaches for addressing antibiotic contamination in water systems.

CRediT authorship contribution statement

Karla V.L. Lima: Writing – review & editing, Writing – original draft, Methodology, Investigation, Formal analysis, Data curation, Conceptualization. **Raquel F. Pupo Nogueira:** Writing – review & editing, Supervision, Funding acquisition, Formal analysis. **Érika M.L. Sousa:** Writing – review & editing, Methodology, Investigation, Formal analysis. **Mário M.Q. Simões:** Writing – review & editing, Supervision, Methodology, Formal analysis. **Diana L.D. Lima:** Writing – review & editing, Supervision, Resources, Methodology, Funding acquisition, Formal analysis, Conceptualization. **Vânia Calisto:** Writing – review & editing, Supervision, Resources, Methodology, Funding acquisition, Formal analysis, Conceptualization.

Declaration of competing interest

The authors declare that they have no known competing financial interests or personal relationships that could have appeared to influence the work reported in this paper.

Acknowledgments

The authors would like to thank the Coordination for the Improvement of Higher Education Personnel (CAPES) for the scholarship granted to K.V.L. Lima under the CAPES-PrInt Program, process number 88887.310463/2018–00, Mobility number 88887.695917/2022–00. É. M.L Sousa thanks support by Fundação para a Ciência e a Tecnologia (FCT) PhD Grant (2020.05390.BD). Diana L.D. Lima thanks support by Fundação para a Ciência e a Tecnologia (FCT) to the SOLCAT research project (2023.12723.PEX, https://doi.org/10.54499/2023.12723.PEX) The Coimbra Health School is also acknowledged for funding the SolarClean project within the call I^2D: Igniting Interdisciplinarity. Financial support to CESAM (UID Centro de Estudos do Ambiente e Mar + LA/P/0094/2020), to LAQV-REQUIMTE (UIDP/50006/2020 + UIDB/50006/2020) and to H&TRC (UIDP/05608/2020 (https://doi.org/10.54499/UIDP/05608/2020) + UIDB/05608/2020 (https://doi.org/10.54499/UIDB/05608/2020)) by FCT/MCTES, through national funds, is also acknowledged. In addition, the authors thank LNNano/CNPEM for the use of XPS (proposal XPS- 20233169) and Peter Hammer for the treatment and analysis of the XPS results. Finally, they extend their gratitude to Mónica Válega for the analysis performed on the UHPLC-MS/MS.

Supplementary materials

Supplementary material associated with this article can be found, in the online version, at doi:10.1016/j.watres.2025.123679.

Data availability

Data will be made available on request.

References

Ahmed, M.B., Zhou, J.L., Ngo, H.H., Guo, W., 2015. Adsorptive removal of antibiotics from water and wastewater: Progress and challenges. Science of the Total Environment 532, 112–126. https://doi.org/10.1016/j.scitotenv.2015.05.130.

Badmus, K.O., Tijani, J.O., Massima, E., Petrik, L., 2018. Treatment of persistent organic pollutants in wastewater using hydrodynamic cavitation in synergy with advanced oxidation process. Environmental Science and Pollution Research 25, 7299–7314. https://doi.org/10.1007/s11356-017-1171-z.

Bajpai, P., 2015. Management of Pulp and Paper Mill Waste. Springer International Publishing, Cham. https://doi.org/10.1007/978-3-319-11788-1.

Behnajady, M.A., Modirshahla, N., Ghanbary, F., 2007. A kinetic model for the decolorization of C.I. Acid Yellow 23 by Fenton process. J. Hazard. Mater. 148, 98–102. https://doi.org/10.1016/j.jhazmat.2007.02.003.

Behrouzeh, M., Abbasi, M., Osfouri, S., Dianat, M.J., 2020. Treatment of DMSO and DMAC wastewaters of various industries by employing Fenton process: Process performance and kinetics study. J. Environ. Chem. Eng. 8, 103597. https://doi.org/10.1016/j.jece.2019.103597.

Bokare, A.D., Choi, W., 2014. Review of iron-free Fenton-like systems for activating H 2 O 2 in advanced oxidation processes. J. Hazard. Mater. 275, 121–135. https://doi.org/10.1016/j.jhazmat.2014.04.054.

Bokhary, A., Tikka, A., Leitch, M., Liao, B., 2018. Membrane fouling prevention and control strategies in pulp and paper industry applications: a review. Journal of Membrane Science and Research 4, 181–197. https://doi.org/10.22079/JMSR.2018.83337.1185.

Brazil, T.R., Gonçalves, M., dos Anjos, E.G.R., de Oliveira Junior, M.S., MC, Rezende, 2022. Microwave-assisted production of activated carbon in an adapted domestic oven from lignocellulosic waste. BioMass Convers. Biorefin. https://doi.org/10.1007/s13399-021-02192-4.

Cai, Q., Hu, J., 2017. Decomposition of sulfamethoxazole and trimethoprim by continuous UVA/LED/TiO2 photocatalysis: decomposition pathways, residual antibacterial activity and toxicity. J. Hazard. Mater. 323, 527–536. https://doi.org/10.1016/j.jhazmat.2016.06.006.

Cao, K.L.A., Kitamoto, Y., Iskandar, F., Ogi, T., 2021. Sustainable porous hollow carbon spheres with high specific surface area derived from Kraft lignin. Advanced Powder Technology 32, 2064–2073. https://doi.org/10.1016/j.apt.2021.04.012.

Chai, F., Li, K., Song, C., Guo, X., 2016. Synthesis of magnetic porous Fe3O4/C/Cu2O composite as an excellent photo-Fenton catalyst under neutral condition. J. Colloid. Interface Sci. 475, 119–125. https://doi.org/10.1016/j.jcis.2016.04.047.

Chen, J., Hu, J., Lin, Y., Liu, X., Liang, J., Zhang, K., et al., 2024. Visible light-driven Cl-g-C3N4 activated peroxydisulfate process for TMP efficient degradation in a wide pH range. J. Water. Process. Eng. 59. https://doi.org/10.1016/j.jwpe.2024.105056.

De Jesus, J.H.F., Lima, K.V.L., 2022. Pupo Nogueira RF. Copper-containing magnetite supported on natural clay as a catalyst for heterogeneous photo-Fenton degradation of antibiotics in WWTP effluent. J. Environ. Chem. Eng. 10, 107765. https://doi.org/10.1016/j.jece.2022.107765.

de Jesus, J.H.F., Lima, K.V.L., Hammer, P., Nogueira, R.F.P., 2023. Wastewater sludge recycling: An efficient catalyst for photo-Fenton degradation of antibiotics and effluent disinfection. Chemical Engineering Journal 467, 143380. https://doi.org/10.1016/j.cej.2023.143380.

EC, 2022. Commission Implementing Decision (EU) 2022/1307 of 22 July 2022 establishing a watch list of substances for Union-wide monitoring in the field of water policy pursuant to Directive 2008/105/EC of the European Parliament and of the Council. Official Journal of the European Union 65, 117.

Fan, G., Ning, R., Yan, Z., Luo, J., Du, B., Zhan, J., et al., 2021. Double photoelectron-transfer mechanism in Ag−AgCl/WO3/g-C3N4 photocatalyst with enhanced visible-light photocatalytic activity for trimethoprim degradation. J. Hazard. Mater. 403. https://doi.org/10.1016/j.jhazmat.2020.123964.

Finlayson-Pitts B.J., Pitts Jr J.N. Applications of Atmospheric Chemistry. 2000.

Gómez-Ramos, M del M, Mezcua, M., Agüera, A., Fernández-Alba, A.R., Gonzalo, S., Rodríguez, A., et al., 2011. Chemical and toxicological evolution of the antibiotic sulfamethoxazole under ozone treatment in water solution. J. Hazard. Mater. 192, 18–25. https://doi.org/10.1016/j.jhazmat.2011.04.072.

Gao, J., Wu, S., Han, Y., Tan, F., Shi, Y., Liu, M., et al., 2018. 3D mesoporous CuFe2O4 as a catalyst for photo-Fenton removal of sulfonamide antibiotics at near neutral pH. J. Colloid. Interface Sci. 524, 409–416. https://doi.org/10.1016/j.jcis.2018.03.112.

Gao, L., Mao, Q., Luo, S., Cao, L., Xie, X., Yang, Y., et al., 2020. Experimental and theoretical insights into kinetics and mechanisms of hydroxyl and sulfate radicals-mediated degradation of sulfamethoxazole: Similarities and differences. Environmental Pollution 259, 113795. https://doi.org/10.1016/j.envpol.2019.113795.

Gmurek, M., Horn, H., Majewsky, M., 2015. Phototransformation of sulfamethoxazole under simulated sunlight: Transformation products and their antibacterial activity toward Vibrio fischeri. Science of the Total Environment 538, 58–63. https://doi.org/10.1016/j.scitotenv.2015.08.014.

Hasija, V., Singh, P., Thakur, S., Stando, K., Nguyen, V.H., Van, Le Q, et al., 2022. Oxygen doping facilitated N-vacancies in g-C3N4 regulates electronic band gap structure for trimethoprim and Cr (VI) mitigation: Simulation studies and photocatalytic degradation pathways. Appl. Mater. Today 29. https://doi.org/10.1016/j.apmt.2022.101676.

He, Z., Xu, X., Wang, B., Lu, Z., Shi, D., Wu, W., 2022. Evaluation of iron-loaded granular activated carbon used as heterogeneous fenton catalyst for degradation of tetracycline. J. Environ. Manage 322, 116077. https://doi.org/10.1016/j.jenvman.2022.116077.

Huang, Y., Yang, J., 2021. Degradation of sulfamethoxazole by the heterogeneous Fenton-like reaction between gallic acid and ferrihydrite. Ecotoxicol. Environ. Saf. 226, 112847. https://doi.org/10.1016/j.ecoenv.2021.112847.

Huang, Y., Xie, Q., Wang, H., Nawaz, M.I., Zhang, H., Song, S., et al., 2024. Degradation of trimethoprim in the simulated solar light/periodate system: Process and mechanism analysis. J. Water. Process. Eng. 57. https://doi.org/10.1016/j.jwpe.2023.104726.

Hussain, S., Aneggi, E., Goi, D., 2021. Catalytic activity of metals in heterogeneous Fenton-like oxidation of wastewater contaminants: a review. Environ. Chem. Lett. 19, 2405–2424. https://doi.org/10.1007/s10311-021-01185-z.

Jaafarzadeh, N., Kakavandi, B., Takdastan, A., Kalantary, R.R., Azizi, M., Jorfi, S., 2015. Powder activated carbon/Fe3O4 hybrid composite as a highly efficient heterogeneous catalyst for Fenton oxidation of tetracycline: Degradation mechanism and kinetic. RSC. Adv. 5, 84718–84728. https://doi.org/10.1039/c5ra17953j.

Jaria, G., Silva, C.P., Oliveira, J.A.B.P., Santos, S.M., Gil, M.V., Otero, M., et al., 2019. Production of highly efficient activated carbons from industrial wastes for the removal of pharmaceuticals from water—A full factorial design. J. Hazard. Mater. 370, 212–218. https://doi.org/10.1016/j.jhazmat.2018.02.053.

Jewell, K.S., Castronovo, S., Wick, A., Falås, P., Joss, A., Ternes, T.A., 2016. New insights into the transformation of trimethoprim during biological wastewater treatment. Water. Res. 88, 550–557. https://doi.org/10.1016/j.watres.2015.10.026.

Jiang, Y., Ran, J., Mao, K., Yang, X., Zhong, L., Yang, C., et al., 2022. Recent progress in Fenton/Fenton-like reactions for the removal of antibiotics in aqueous environments. Ecotoxicol. Environ. Saf. 236, 113464. https://doi.org/10.1016/j.ecoenv.2022.113464.

Kim, W., Suh, C.Y., Cho, S.W., Roh, K.M., Kwon, H., Song, K., et al., 2012. A new method for the identification and quantification of magnetite-maghemite mixture using conventional X-ray diffraction technique. Talanta 94, 348–352. https://doi.org/10.1016/j.talanta.2012.03.001.

Labiadh, L., Ammar, S., Kamali, A.R., 2019. Oxidation/mineralization of AO7 by electro-Fenton process using chalcopyrite as the heterogeneous source of iron and copper catalysts with enhanced degradation activity and reusability. Journal of Electroanalytical Chemistry 853, 113532. https://doi.org/10.1016/j.jelechem.2019.113532.

Le, Na PT, NDK, Tuyen, Dang, B.T, 2024. Sorption of four antibiotics onto pristine biochar derived from macadamia nutshell. Bioresour. Technol. 394, 130281. https://doi.org/10.1016/j.biortech.2023.130281.

Li, Y., Cheng, H., 2021. Chemical kinetic modeling of organic pollutant degradation in Fenton and solar photo-Fenton processes. J. Taiwan. Inst. Chem. Eng. 123, 175–184. https://doi.org/10.1016/j.jtice.2021.05.011.

Li, T., Chen, Y., Wang, X., Liang, J., Zhou, L., 2021. Modifying organic carbon in Fe3O4-loaded schwertmannite to improve heterogeneous Fenton activity through accelerating Fe(II) generation. Appl. Catal. B 285, 119830. https://doi.org/10.1016/j.apcatb.2020.119830.

Li, S., Yang, Y., Zheng, H., Zheng, Y., Jing, T., Ma, J., et al., 2022. Advanced oxidation process based on hydroxyl and sulfate radicals to degrade refractory organic pollutants in landfill leachate. Chemosphere 297, 134214. https://doi.org/10.1016/j.chemosphere.2022.134214.

Li, Y., Shang, H., Cao, Y., Yang, C., Feng, Y., Yu, Y., 2022. Quantification of adsorption mechanisms distribution of sulfamethoxazole onto biochar by competition relationship in a wide pH range. J. Environ. Chem. Eng. 10, 108755. https://doi.org/10.1016/j.jece.2022.108755.

Li, J., Li, Y., Maryam, B., Chen, X., Zong, Y., Tu, J., et al., 2023. Microplastic aging alters the adsorption-desorption behaviors of sulfamethoxazole in marine animals: a study in simulated biological liquids. Mar. Pollut. Bull. 195, 115473. https://doi.org/10.1016/j.marpolbul.2023.115473.

Li, Y., Li, X., Wang, B., 2023. Precisely introducing active sites into NU-1000 through linker incorporation for degrading sulfamethoxazole under visible-light photo-Fenton process. Sep. Purif. Technol. 309, 123013. https://doi.org/10.1016/j.seppur.2022.123013.

Li, X., Zhao, Y., Yuan, T., Zhang, Y., Shu, X., Lu, X., 2024. Periodate activation by MnFe2O4 spinel for sulfamethoxazole degradation: Iodate radical dominance, degradation pathway, DFT calculation and toxicity assessment. Sep. Purif. Technol. 347. https://doi.org/10.1016/j.seppur.2024.127553.

Lima, M.J., Silva, C.G., Silva, A.M.T., Lopes, J.C.B., Dias, M.M., Faria, J.L., 2017. Homogeneous and heterogeneous photo-Fenton degradation of antibiotics using an innovative static mixer photoreactor. Chemical Engineering Journal 310, 342–351. https://doi.org/10.1016/j.cej.2016.04.032.

Liu, S.Q., Feng, L.R., Xu, N., Chen, Z.G., Wang, X.M., 2012. Magnetic nickel ferrite as a heterogeneous photo-Fenton catalyst for the degradation of rhodamine B in the presence of oxalic acid. Chemical Engineering Journal 203, 432–439. https://doi.org/10.1016/j.cej.2012.07.071.

Liu, Q., Li, M., Liu, X., Zhang, Q., Liu, R., Wang, Z., et al., 2018. Removal of sulfamethoxazole and trimethoprim from reclaimed water and the biodegradation mechanism. Front. Environ. Sci. Eng. 12. https://doi.org/10.1007/s11783-018-1048-5.

Liu, L., Yu, R., Zhao, S., Cao, X., Zhang, X., Bai, S., 2023. Heterogeneous Fenton system driven by iron-loaded sludge biochar for sulfamethoxazole-containing wastewater treatment. J. Environ. Manage 335, 117576. https://doi.org/10.1016/j.jenvman.2023.117576.

Liu, G., Liu, M., Shi, H., Jia, H., Zou, H., Tao, N., 2023. Efficient electrochemical decomposition of sulfamethoxazole using a novel free-standing TiN anode. Sustainable Horizons 7. https://doi.org/10.1016/j.horiz.2023.100059.

Marsh, H., Rand, B., 1970. The characterization of microporous carbons by means of the dubinin-radushkevich equation. J. Colloid. Interface Sci. 33, 101–116. https://doi.org/10.1016/0021-9797(70)90077-9.

Martínez-Costa, J.I., Rivera-Utrilla, J., Leyva-Ramos, R., Sánchez-Polo, M., Velo-Gala, I., Mota, A.J., 2018. Individual and simultaneous degradation of the antibiotics sulfamethoxazole and trimethoprim in aqueous solutions by Fenton, Fenton-like and photo-Fenton processes using solar and UV radiations. J. Photochem. Photobiol. a Chem. 360, 95–108. https://doi.org/10.1016/j.jphotochem.2018.04.014.

Mo, C.C., Tian, F.X., Xu, B., Wang, J., Gao, Y.Q., Bi, D.S., et al., 2024. Efficient trimethoprim removal via cooperation of radical and non-radical pathways in UV/peroxymonosulfate: Kinetics, mechanisms and disinfection by-products-associated risks. J. Environ. Chem. Eng. 12. https://doi.org/10.1016/j.jece.2024.112368.

Nawaz, M., Shahzad, A., Tahir, K., Kim, J., Moztahida, M., Jang, J., et al., 2020. Photo-Fenton reaction for the degradation of sulfamethoxazole using a multi-walled carbon nanotube-NiFe2O4 composite. Chemical Engineering Journal 382, 123053. https://doi.org/10.1016/j.cej.2019.123053.

Nogueira, R.F.P., Oliveira, M.C., Paterlini, W.C., 2005. Simple and fast spectrophotometric determination of H2O 2 in photo-Fenton reactions using metavanadate. Talanta 66, 86–91. https://doi.org/10.1016/j.talanta.2004.10.001.

Özel Duygan, B.D., Udert, K.M., Remmele, A., McArdell, C.S., 2021. Removal of pharmaceuticals from human urine during storage, aerobic biological treatment, and activated carbon adsorption to produce a safe fertilizer. Resour. Conserv. Recycl. 166, 105341. https://doi.org/10.1016/j.resconrec.2020.105341.

Pan, L., Cao, Y., Zang, J., Huang, Q., Wang, L., Zhang, Y., et al., 2019. Preparation of iron-loaded granular activated carbon catalyst and its application in tetracycline antibiotic removal from aqueous solution. Int. J. Environ. Res. Public Health 16, 5–7. https://doi.org/10.3390/ijerph16132270.

Pereira, D., Gil, M.V, Esteves, V.I., Silva, N.J.O., Otero, M., Calisto, V., 2023. Ex-situ magnetic activated carbon for the adsorption of three pharmaceuticals with distinct physicochemical properties from real wastewater. J. Hazard. Mater. 443. https://doi.org/10.1016/j.jhazmat.2022.130258.

Pereira, D., Gil, M.V, Esteves, V.I., Silva, N.J.O., Otero, M., Calisto, V., 2025. One-step microwave conversion of paper mill sludge into magnetic activated carbon for the removal of pharmaceuticals from water. J. Water. Process. Eng. 69. https://doi.org/10.1016/j.jwpe.2024.106766.

Psutka, J.M., Dion-Fortier, A., Dieckmann, T., Campbell, J.L., Segura, P.A., Hopkins, W. S., 2018. Identifying Fenton-Reacted Trimethoprim Transformation Products Using Differential Mobility Spectrometry. Anal. Chem. 90, 5352–5357. https://doi.org/10.1021/acs.analchem.8b00484.

Rocha, L.S., Pereira, D., Sousa, É., Otero, M., Esteves, V.I., Calisto, V., 2020. Recent advances on the development and application of magnetic activated carbon and char for the removal of pharmaceutical compounds from waters: a review. Science of the Total Environment 718. https://doi.org/10.1016/j.scitotenv.2020.137272.

Salvador, F., Martin-Sanchez, N., Sanchez-Hernandez, R., Sanchez-Montero, M.J., Izquierdo, C., 2015. Regeneration of carbonaceous adsorbents. Part II: Chemical, Microbiological and Vacuum Regeneration. Microporous and Mesoporous Materials 202, 277–296. https://doi.org/10.1016/j.micromeso.2014.08.019.

Samy, M., Ibrahim, M.G., Gar Alalm, M., Fujii, M., Ookawara, S., Ohno, T., 2020. Photocatalytic degradation of trimethoprim using S-TiO2 and Ru/WO3/ZrO2 immobilized on reusable fixed plates. J. Water. Process. Eng. 33. https://doi.org/10.1016/j.jwpe.2019.101023.

Sanusi, I.O., Olutona, G.O., Wawata, I.G., Onohuean, H., 2023. Occurrence, environmental impact and fate of pharmaceuticals in groundwater and surface water: a critical review. Environmental Science and Pollution Research 30, 90595–90614. https://doi.org/10.1007/s11356-023-28802-4.

Seidmohammadi, A., Vaziri, Y., Dargahi, A., Nasab, H.Z., 2021. Improved degradation of metronidazole in a heterogeneous photo-Fenton oxidation system with PAC/Fe3O4 magnetic catalyst: biodegradability, catalyst specifications, process optimization, and degradation pathway. BioMass Convers. Biorefin. https://doi.org/10.1007/s13399-021-01668-7.

Serna-Galvis, E.A., Botero-Coy, A.M., Martínez-Pachón, D., Moncayo-Lasso, A., Ibáñez, M., Hernández, F., et al., 2019. Degradation of seventeen contaminants of emerging concern in municipal wastewater effluents by sonochemical advanced oxidation processes. Water. Res. 154, 349–360. https://doi.org/10.1016/j.watres.2019.01.045.

Shang, J.G., Kong, X.R., He, L.L., Li, W.H., Liao, Q.J.H., 2016. Low-cost biochar derived from herbal residue: characterization and application for ciprofloxacin adsorption.

International Journal of Environmental Science and Technology 13, 2449–2458. https://doi.org/10.1007/s13762-016-1075-3.
Singh, S., Kaur, P., Aggarwal, D., Kumar, V., Tikoo, K., Bansal, S., et al., 2022. Polyaniline enwrapped CoFe2O4/g-CN ternary nanocomposite for adsorption driven photocatalytic degradation of explicitly diverse organic pollutants. J. Alloys. Compd. 923, 166255. https://doi.org/10.1016/j.jallcom.2022.166255.
Sirtori, C., Agüera, A., Gernjak, W., Malato, S., 2010. Effect of water-matrix composition on Trimethoprim solar photodegradation kinetics and pathways. Water. Res. 44, 2735–2744. https://doi.org/10.1016/j.watres.2010.02.006.
Song, Y., Li, Y., Chen, X., Meng, C., Ma, S., Li, T., et al., 2023. Simultaneous degradation and separation of antibiotics in sewage effluent by photocatalytic nanofiltration membrane in a continuous dynamic process. Water. Res. 229, 119460. https://doi.org/10.1016/j.watres.2022.119460.
Soriano-Molina, P., De la Obra, I., Miralles-Cuevas, S., Gualda-Alonso, E., Casas López, J. L., Sánchez Pérez, J.A, 2021. Assessment of different iron sources for continuous flow solar photo-Fenton at neutral pH for sulfamethoxazole removal in actual MWWTP effluents. J. Water. Process. Eng. 42. https://doi.org/10.1016/j.jwpe.2021.102109.
Sousa, É.M.L., Otero, M., Rocha, L.S., Gil, M.V, Ferreira, P., Esteves, V.I., et al., 2022. Multivariable optimization of activated carbon production from microwave pyrolysis of brewery wastes - Application in the removal of antibiotics from water. J. Hazard. Mater. 431, 128556. https://doi.org/10.1016/j.jhazmat.2022.128556.
Sousa, É.M.L., Otero, M., Gil, M.V, Ferreira, P., Esteves, V.I., Calisto, V., 2023. Insights into matrix and competitive effects on antibiotics removal from wastewater by activated carbon produced from brewery residues. Environ. Technol. Innov. 30, 103074. https://doi.org/10.1016/j.eti.2023.103074.
Spessato, L., Cazetta, A.L., Melo, S., Pezoti, O., Tami, J., Ronix, A., et al., 2020. Synthesis of superparamagnetic activated carbon for paracetamol removal from aqueous solution. J. Mol. Liq. 300. https://doi.org/10.1016/j.molliq.2019.112282.
Stando, K., Czyż, A., Gajda, M., Felis, E., Bajkacz, S., 2022. Study of the Phytoextraction and Phytodegradation of Sulfamethoxazole and Trimethoprim from Water by Limnobium laevigatum. Int. J. Environ. Res. Public Health 19. https://doi.org/10.3390/ijerph192416994.
Tang, J., Wang, J., 2018. Fenton-like degradation of sulfamethoxazole using Fe-based magnetic nanoparticles embedded into mesoporous carbon hybrid as an efficient catalyst. Chemical Engineering Journal 351, 1085–1094. https://doi.org/10.1016/j.cej.2018.06.169.
Tang, C., Ma, S.Q., Yi, X.H., Wang, C.C., Wang, P., 2023. MIL-88A(Fe)/TCNQ composites for boosted photo-Fenton sulfamethoxazole degradation under LED visible light. Mater. Res. Bull. 160. https://doi.org/10.1016/j.materresbull.2022.112138.
Trovó, A.G., Nogueira, R.F.P., Agüera, A., Sirtori, C., Fernández-Alba, A.R., 2009. Photodegradation of sulfamethoxazole in various aqueous media: Persistence, toxicity and photoproducts assessment. Chemosphere 77, 1292–1298. https://doi.org/10.1016/j.chemosphere.2009.09.065.
Velo-Gala, I., López-Peñalver, J.J., Sánchez-Polo, M., Rivera-Utrilla, J., 2014. Surface modifications of activated carbon by gamma irradiation. Carbon. N. Y. 67, 236–249. https://doi.org/10.1016/j.carbon.2013.09.087.
Voigt, M., Bartels, I., Nickisch-Hartfiel, A., Jaeger, M., 2017. Photoinduced degradation of sulfonamides, kinetic, and structural characterization of transformation products and assessment of environmental toxicity. Toxicol. Environ. Chem. 99, 1304–1327. https://doi.org/10.1080/02772248.2017.1373777.
Wang, S., Wang, J., 2018. Trimethoprim degradation by Fenton and Fe(II)-activated persulfate processes. Chemosphere 191, 97–105. https://doi.org/10.1016/j.chemosphere.2017.10.040.
Wang, A., Li, Y.Y., Estrada, A.L., 2011. Mineralization of antibiotic sulfamethoxazole by photoelectro-Fenton treatment using activated carbon fiber cathode and under UVA irradiation. Appl. Catal. B 102, 378–386. https://doi.org/10.1016/j.apcatb.2010.12.007.
Wang, K., Zhuang, T., Su, Z., Chi, M., Wang, H., 2021. Antibiotic residues in wastewaters from sewage treatment plants and pharmaceutical industries: Occurrence, removal and environmental impacts. Science of the Total Environment 788, 147811. https://doi.org/10.1016/j.scitotenv.2021.147811.
Wang, J., Qin, J., Liu, B., Song, S., 2022. Reaction mechanisms and toxicity evolution of Sulfamethoxazole degradation by CoFe-N doped C as Electro-Fenton cathode. Sep. Purif. Technol. 298, 121655. https://doi.org/10.1016/j.seppur.2022.121655.
Wei, Y., Zhang, L., Liang, B., Cui, H., Shi, K., Liu, Z., et al., 2024. Synergistic Control of Trimethoprim and the Antimicrobial Resistome in Electrogenic Microbial Communities. Environ. Sci. Technol. 58, 2847–2858. https://doi.org/10.1021/acs.est.3c05870.
Yang, Y., Lu, X., Jiang, J., Ma, J., Liu, G., Cao, Y., et al., 2017. Degradation of sulfamethoxazole by UV, UV/H2O2 and UV/persulfate (PDS): Formation of oxidation products and effect of bicarbonate. Water. Res. 118, 196–207. https://doi.org/10.1016/j.watres.2017.03.054.
Yang, Y., Zhang, X., Jiang, J., Han, J., Li, W., Li, X., et al., 2022. Which Micropollutants in Water Environments Deserve More Attention Globally? Environ. Sci. Technol. 56, 13–29. https://doi.org/10.1021/acs.est.1c04250.
Zárate-Guzmán, A.I., González-Gutiérrez, L.V, Ocampo-Pérez, R., Carrasco-Marín, F., Romero-Cano, L.A., 2020. Iron precursor salt effect on the generation of [rad]OH radicals and sulfamethoxazole degradation through a heterogeneous Fenton process using Carbon-Fe catalysts. J. Water. Process. Eng. 36, 101273. https://doi.org/10.1016/j.jwpe.2020.101273.
Zeng, S., Kan, E., 2022. FeCl3-activated biochar catalyst for heterogeneous Fenton oxidation of antibiotic sulfamethoxazole in water. Chemosphere 306, 135554. https://doi.org/10.1016/j.chemosphere.2022.135554.
Zhang, N., Zhou, B., Yuan, R., Wang, F., Chen, H., 2020. Effect of natural organic matter on the ozonation mechanism of trimethoprim in water. Water (Switzerland) 12, 1–15. https://doi.org/10.3390/w12102935.
Zhu, Y., Zhu, R., Xi, Y., Zhu, J., Zhu, G., He, H., 2019. Strategies for enhancing the heterogeneous fenton catalytic reactivity: a review. Appl. Catal. B 255, 117739. https://doi.org/10.1016/j.apcatb.2019.05.041.
Zhu, R., Zhu, Y., Xian, H., Yan, L., Fu, H., Zhu, G., et al., 2020. CNTs/ferrihydrite as a highly efficient heterogeneous Fenton catalyst for the degradation of bisphenol A: The important role of CNTs in accelerating Fe(III)/Fe(II) cycling. Appl. Catal. B 270, 118891. https://doi.org/10.1016/j.apcatb.2020.118891.